Design of the Symmetrical OTA

For a Generic 180nm Bulk CMOS Process (Version 2)

Christian Enz (christian.enz@epfl.ch)

2025-07-25

Table of contents

1 Introduction

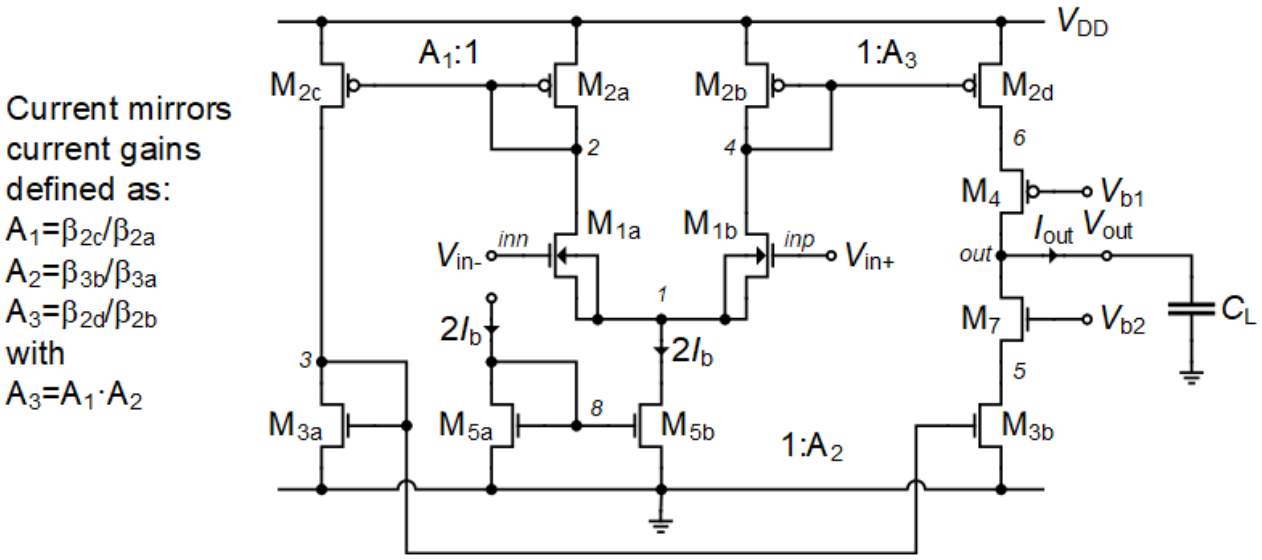

Figure 1.1: Schematic of the symmetrical differential OTA.

> **Note**
>
> Note that all nMOS transistors in Figure 1.1 have an odd number and all the pMOS transistors an even number which explains the numbering process (this is the reason why there is no M_6 transistor!).

This notebook presents the analysis, design and simulation of the symmetrical cascode OTA which schematic is presented in Figure 1.1 [1]. The design phase is using the sEKV model and the inversion coefficient approach [2], [3], [4]. The symmetrical OTA is a single-stage OTA having the dominant pole set by the load capacitance. It therefore doesn't require any compensation capacitance but can still achieve the gain of a two-stage OTA thanks to the cascode stages at the output at much lower current consumption. We will see below that in differential mode the effects of the source transconductances on the common source node voltage are actually canceled. In order to minimize the V_{GS} voltage of M_{1a}-M_{1b}, we have chosen to put M_{1a}-M_{1b} in a separate well at the cost of a larger area.

We will start with a detailed analysis of the OTA which will allow to derive all the design equations that will be used in the design phase. The OTA is then designed for a given set of specifications for a generic 180 nm bulk CMOS technology. The design is then validated by simulations with ngspice [5] using the EKV 2.6 compact model [6] [7] [8] with parameters corresponding to a generic 180 nm bulk CMOS technology [9] [10].

We now start with the small-signal analysis.

2 Analysis

2.1 Small-signal analysis

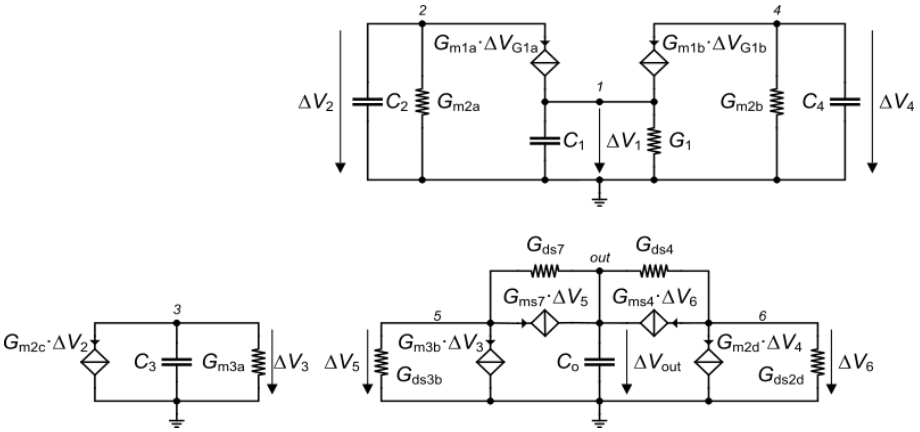

Figure 2.1: Small-signal schematic of the symmetrical cascode OTA.

The small-signal schematic of the symmetrical OTA of Figure 1.1 is shown in Figure 2.1. The design of the symmetrical cascode OTA is similar to the design of the simple OTA, except that there are now more parasitic poles appearing at the various current mirror nodes. The small-signal output voltage in open-loop is given by

$$\Delta V_{out} = \frac{A_{dc}}{1+s\,\tau_0}\cdot\left[\frac{\Delta V_{in+}}{1+s\,\tau_{p4}} - \frac{\Delta V_{in-}}{(1+s\,\tau_{p2})(1+s\,\tau_{p3})}\right. \tag{2.1}$$

$$\left. -\frac{\Delta V_{in+}+\Delta V_{in-}}{2(1+s\,\tau_{p1})}\cdot\left(\frac{1}{1+s\,\tau_{p4}} - \frac{1}{(1+s\,\tau_{p2})(1+s\,\tau_{p3})}\right)\right] \tag{2.2}$$

where

$$A_{dc} = \frac{G_m}{G_o}, \tag{2.3}$$

$$G_m = A_3\cdot G_{m1}, \tag{2.4}$$

$$G_o = \frac{G_{ds3b}\,G_{ds7}}{G_{ms7}} + \frac{G_{ds2d}\,G_{ds4}}{G_{ms4}}, \tag{2.5}$$

$$\tau_0 = \frac{C_{out}}{G_o}, \tag{2.6}$$

$$C_{out} = C_L + C_o, \tag{2.7}$$

$$\tau_{p1} = \frac{C_1}{2G_{m1}}, \tag{2.8}$$

$$\tau_{p2} = \frac{C_2}{G_{m2}}, \tag{2.9}$$

$$\tau_{p3} = \frac{C_3}{G_{m3}}, \tag{2.10}$$

$$\tau_{p4} = \frac{C_4}{G_{m2}}. \tag{2.11}$$

C_1, C_2 and C_3 are the total parasitic capacitances at the current mirrors nodes 1, 2 and 3.

The unity-gain frequency or gain-bandwidth product is defined as $\omega_u = 1/\tau_u \triangleq A_{dc}/\tau_0 = G_m/C_{out}$. In most practical cases, we usually have $\tau_0 \gg \tau_{p2}, \tau_{p3}, \tau_{p4} > \tau_{p1}$.

For a differential input voltage $\Delta V_{id} = \Delta V_{in+} - \Delta V_{in-}$ with a constant common-mode voltage V_{ic} and hence $\Delta V_{ic} = (\Delta V_{in+} + \Delta V_{in-})/2 = 0$, $\Delta V_{in+} = -\Delta V_{in-} = \Delta V_{id}/2$, the differential mode small-signal open-loop gain reduces to

$$A_{dm}(s) \triangleq \frac{\Delta V_{out}}{\Delta V_{id}} = \frac{1}{2} \cdot \frac{A_{dc}}{1 + s\,\tau_0} \cdot \left[\frac{1}{1 + s\,\tau_{p4}} - \frac{1}{(1 + s\,\tau_{p2})(1 + s\,\tau_{p3})} \right]. \tag{2.12}$$

The small-signal output voltage ΔV_{out} can also be written as

$$\Delta V_{out} = \frac{A_{dc}}{1 + s\,\tau_0} \cdot \left[F(s) \cdot \Delta V_{in+} - G(s) \cdot \Delta V_{in-} \right], \tag{2.13}$$

where

$$F(s) = \frac{1}{1 + s\,\tau_{p4}} - \frac{1}{2} \frac{1}{1 + s\,\tau_{p1}} \cdot \left[\frac{1}{1 + s\,\tau_{p4}} - \frac{1}{(1 + s\,\tau_{p2})(1 + s\,\tau_{p3})} \right], \tag{2.14}$$

$$G(s) = \frac{1}{(1 + s\,\tau_{p2})(1 + s\,\tau_{p3})} + \frac{1}{2} \frac{1}{1 + s\,\tau_{p1}} \cdot \left[\frac{1}{1 + s\,\tau_{p4}} - \frac{1}{(1 + s\,\tau_{p2})(1 + s\,\tau_{p3})} \right]. \tag{2.15}$$

From (2.13) we see that the time constant τ_0 introduces a $-90°$ phase shift. Hence if the desired phase margin is at least $60°$, the additional phase shift introduced by the smaller time constants τ_{p1}, τ_{p2}, τ_{p3} and τ_{p4} should not exceed $30°$. In this range, the product $(1 + s\,\tau_{p1})(1 + s\,\tau_{p2})(1 + s\,\tau_{p3})(1 + s\,\tau_{p4})$ can be expanded and approximated by neglecting all the order terms higher than the first order term in s

$$\prod_{k=1}^{4} (1 + s\,\tau_{pk}) \cong 1 + s \sum_{k=1}^{4} \tau_{pk}. \tag{2.16}$$

The above approximation gives a good estimation of the phase shift ϕ for $\phi < 30°$, which correspond to the following frequency range

$$\omega \leq \left(2 \sum_{k=1}^{4} \tau_{pk} \right)^{-1}. \tag{2.17}$$

Using the above approximation leads to

$$F(s) \cong G(s) \cong \frac{1 + s\,\tau_n}{1 + s\,\tau_d}, \tag{2.18}$$

where

$$\tau_n = \tau_{p1} + \frac{\tau_{p2} + \tau_{p3} + \tau_{p4}}{2}, \tag{2.19}$$

$$\tau_d = \tau_{p1} + \tau_{p2} + \tau_{p3} + \tau_{p4}. \tag{2.20}$$

For $\omega \leq 1/(2\tau_d)$, the above expression can be further simplified considering that

$$\frac{1 + s\,\tau_n}{1 + s\,\tau_d} \cong \frac{1}{1 + s\,(\tau_d - \tau_n)} \tag{2.21}$$

where

$$\tau_d - \tau_n = \frac{\tau_{p2} + \tau_{p3} + \tau_{p4}}{2} = \frac{\tau_p}{2}. \tag{2.22}$$

$F(s)$ and $G(s)$ become

$$F(s) \cong G(s) \cong \frac{1}{1 + s\,\frac{\tau_p}{2}}, \tag{2.23}$$

which is valid for $\omega \leq 1/(2\tau_d) = 1/(2(\tau_{p2} + \tau_p))$.

The simplified differential transfer function is then given by

$$A_{dm}(s) \cong \frac{A_{dc}}{(1 + s\,\tau_0)\,(1 + s\,\frac{\tau_p}{2})} = \frac{A_{dc}}{\left(1 + \frac{s}{\omega_0}\right)\left(1 + \frac{s}{\omega_p}\right)} \tag{2.24}$$

with $\omega_0 \triangleq 1/\tau_0$ and $\omega_p \triangleq 2/\tau_p$ where it is assumed that $\tau_p = \tau_{p2} + \tau_{p3} + \tau_{p4} \ll \tau_0$. $\omega_0 \triangleq 1/\tau_0 \ll \omega_p$ is the dominant pole which is set by the load capacitance at the OTA output, whereas $\omega_p \triangleq 2/\tau_p$ represents the non-dominant pole related to all the time constants due to the parasitic capacitances at the current mirror nodes.

The transfer function can be further simplified as

$$A_{dm}(s) \cong \frac{1}{s\,\tau_u\,(1 + s\,\frac{\tau_p}{2})} = \frac{1}{\frac{s}{\omega_u}\left(1 + \frac{s}{\omega_p}\right)} \tag{2.25}$$

where $\omega_u = 1/\tau_u = A_{dc} \cdot \omega_0 = G_m/C_{out}$ is the unity gain frequency or the gain-bandwidth product GBW which is set by the OTA transconductance G_m and the load capacitance C_{out}.

2.2 Noise analysis

We have seen that the noise of the cascode transistors M_4 and M_7 can actually be neglected. Remembering that $A_3 = A_1 \cdot A_2$, the PSD of the output noise current is given by

$$S_{I_{nout}} = A_3^2\,(S_{I_{n1a}} + S_{I_{n1b}} + S_{I_{n2a}} + S_{I_{n2b}}) + A_2^2\,(S_{I_{n2c}} + S_{I_{n3a}}) + S_{I_{n2d}} + S_{I_{n3b}} \tag{2.26}$$

or if we express the output PSD in terms of the output noise conductance

$$S_{I_{nout}} = 4kT \cdot G_{nout} \tag{2.27}$$

where

$$G_{nout} = 2A_3^2 \cdot (G_{n1} + G_{n2}) + A_2^2 \cdot (G_{n2c} + G_{n3a}) + G_{n2d} + G_{n3b} \tag{2.28}$$

where we have assumed that M_{1a} and M_{1b} and M_{2a} and M_{2b} are identical. The G_{ni} are given by

$$G_{ni} = \gamma_{ni} \cdot G_{mi} + G_{mi}^2 \cdot \frac{\rho_i}{W_i\,L_i\,f} \qquad \text{for all transistors.} \tag{2.29}$$

The input-referred noise resistance R_{nin} is then given by

$$R_{nin} \triangleq \frac{G_{nout}}{A_3^2 \cdot G_{m1}^2} = \frac{2(G_{n1} + G_{n2})}{G_{m1}^2} + \frac{G_{n2c} + G_{n3a}}{A_1^2 \cdot G_{m1}^2} + \frac{G_{n2d} + G_{n3b}}{A_3^2 \cdot G_{m1}^2} \tag{2.30}$$

where we have used $A_3 = A_1 \cdot A_2$. As expected, we see that the noise contribution to the input-referred noise of M_{2d} and M_{3b} is divided by A_3^2 and that from M_{2c} and M_{3a} is divided by A_1^2.

We now look at the input-referred thermal and flicker noise separately.

2.2.1 Input-referred thermal noise

The input-referred thermal noise resistance is given by

$$R_{nth} = \frac{2\gamma_{n1}}{G_{m1}} \cdot (1 + \eta_{th}) \tag{2.31}$$

where

$$\eta_{th} = \frac{\gamma_{n2}}{\gamma_{n1}} \frac{G_{m2}}{G_{m1}} + \frac{1}{2A_1^2} \left(\frac{\gamma_{n2c}}{\gamma_{n1}} \frac{G_{m2c}}{G_{m1}} + \frac{\gamma_{n3a}}{\gamma_{n1}} \frac{G_{m3a}}{G_{m1}} \right) \tag{2.32}$$

$$+ \frac{1}{2A_3^2} \left(\frac{\gamma_{n2d}}{\gamma_{n1}} \frac{G_{m2d}}{G_{m1}} + \frac{\gamma_{n3b}}{\gamma_{n1}} \frac{G_{m3b}}{G_{m1}} \right) \tag{2.33}$$

represents the contributions to the input-referred thermal noise of the current mirrors relative to that of the differential pair. Now $G_{m2c} = A_1 \cdot G_{m2a} = A_1 \cdot G_{m2}$, $G_{m3b} = A_2 \cdot G_{m3a} = A_2 \cdot G_{m3}$ and $G_{m2d} = A_3 \cdot G_{m2b} = A_3 \cdot G_{m2}$, and assuming that $\gamma_{n2a} = \gamma_{n2b} \cong \gamma_{n2c} \cong \gamma_{n2d} = \gamma_{n2}$ and $\gamma_{n3a} \cong \gamma_{n3b} = \gamma_{n3}$, then η_{th} reduces to

$$\eta_{th} = \frac{\gamma_{n2}}{2\gamma_{n1}} \frac{G_{m2}}{G_{m1}} \left(2 + \frac{1}{A_1} + \frac{1}{A_3} \right) + \frac{1}{2A_1^2} \frac{\gamma_{n3}}{\gamma_{n1}} \frac{G_{m3}}{G_{m1}} \left(1 + \frac{1}{A_2} \right) \tag{2.34}$$

In the case of unity current gains $A_1 = A_2 = A_3 = 1$, η_{th} simplifies further to

$$\eta_{th} = 2\frac{\gamma_{n2}}{\gamma_{n1}} \frac{G_{m2}}{G_{m1}} + \frac{\gamma_{n3}}{\gamma_{n1}} \frac{G_{m3}}{G_{m1}} \tag{2.35}$$

Of course in the design process, we will try to minimize η_{th} so that the dominant contribution to the input-referred thermal noise comes from the differential pair M_{1a}-M_{1b}.

We can also introduce the OTA thermal noise excess factor as

$$\gamma_{ota} \triangleq G_m \cdot R_{nth}, \tag{2.36}$$

where $G_m = A_3 \cdot G_{m1}$ is the OTA transconductance. This results in

$$\gamma_{ota} = 2A_3 \cdot \gamma_{n1} \cdot (1 + \eta_{th}). \tag{2.37}$$

We see that introducing some current gains larger than one in the current mirrors allows to reduce the contributions of transistors M_{2c}-M_{2d} and M_{3a}-M_{3b}, but on the other hand increases the contribution of the differential pair and hence degrading (i.e. increasing) the OTA thermal noise excess factor γ_{ota}.

For $G_{m1} \gg G_{m2}$ and $G_{m1} \gg G_{m3}$, the noise is dominated by the differential pair and

$$\gamma_{ota} \cong 2A_3 \cdot \gamma_{n1}. \tag{2.38}$$

For unity current gains $A_1 = A_2 = A_3 = 1$, the OTA thermal noise excess factor γ_{ota} reduces to

$$\gamma_{ota} \cong 2\gamma_{n1}. \tag{2.39}$$

2.2.2 Input-referred flicker noise

The input-referred flicker noise resistance is given by

$$f \cdot R_{nfl} = \frac{2\rho_n}{W_1 L_1} + \rho_p \left(\frac{G_{m2}}{G_{m1}} \right)^2 \left(\frac{2}{W_2 L_2} + \frac{1}{W_{2c} L_{2c}} + \frac{1}{W_{2d} L_{2d}} \right) \tag{2.40}$$

$$+ \frac{\rho_n}{A_1^2} \left(\frac{G_{m3}}{G_{m1}} \right)^2 \left(\frac{1}{W_{3a} L_{3a}} + \frac{1}{W_{3b} L_{3b}} \right) \tag{2.41}$$

which can be written as

$$R_{nfl} = \frac{2\rho_n}{W_1 L_1 f} \cdot (1 + \eta_{fl}) \tag{2.42}$$

where η_{fl} represents the contributions to the input-referred flicker noise resistance of the current mirrors relative to that of the differential pair

$$\eta_{fl} = \frac{\rho_p}{2\rho_n} \left(\frac{G_{m2}}{G_{m1}}\right)^2 \left(\frac{2W_1L_1}{W_2L_2} + \frac{W_1L_1}{W_{2c}L_{2c}} + \frac{W_1L_1}{W_{2d}L_{2d}}\right) \tag{2.43}$$

$$+ \frac{1}{2A_1^2} \left(\frac{G_{m3}}{G_{m1}}\right)^2 \left(\frac{W_1L_1}{W_{3a}L_{3a}} + \frac{W_1L_1}{W_{3b}L_{3b}}\right). \tag{2.44}$$

For $A_1 = A_2 = A_3 = 1$, $W_{2a} = W_{2b} = W_{2c} = W_{2d} = W_2$, $L_{2a} = L_{2b} = L_{2c} = L_{2d} = L_2$, $W_{3a} = W_{3b} = W_3$ and $L_{3a} = L_{3b} = L_3$ reduces to

$$\eta_{fl} = 2\frac{\rho_p}{\rho_n} \left(\frac{G_{m2}}{G_{m1}}\right)^2 \frac{W_1L_1}{W_2L_2} + \left(\frac{G_{m3}}{G_{m1}}\right)^2 \frac{W_1L_1}{W_3L_3}. \tag{2.45}$$

Similarly to thermal noise, in the design process we will try to minimize η_{fl} in order to reduce the input-referred flicker noise to the contribution of the differential pair M_{1a}-M_{1b}.

The corner frequency is obtained by equating $R_{nfl(f_k)} = R_{nth}$ resulting in

$$f_k = \frac{\rho_n G_{m1}}{W_1 L_1 \gamma_{n1}} \cdot \frac{1 + \eta_{fl}}{1 + \eta_{th}}. \tag{2.46}$$

2.3 Input-referred offset voltage

The input-referred random offset voltage can be obtained in a similar way than noise. The variance of the input-referred offset voltage is given by

$$\sigma^2_{V_{os}} = \sigma^2_{V_{T1}} \cdot (1 + \xi_{V_T}) + \left(\frac{I_b}{G_{m1}}\right)^2 \cdot \sigma^2_{\beta_1} \cdot (1 + \xi_\beta) \tag{2.47}$$

where ξ_{V_T} represents the V_T-mismatch contributions to the input-referred offset of the current mirrors relative to that of the differential pair

$$\xi_{V_T} = 2\left(\frac{G_{m2}}{G_{m1}}\right)^2 \cdot \frac{\sigma^2_{V_{T2}}}{\sigma^2_{V_{T1}}} + \left(\frac{G_{m3}}{A_1 G_{m1}}\right)^2 \cdot \frac{\sigma^2_{V_{T3}}}{\sigma^2_{V_{T1}}} \tag{2.48}$$

and ξ_β represents the β-mismatch contributions to the input-referred offset of the current mirrors relative to that of the differential pair

$$\xi_\beta = 2\frac{\sigma^2_{\beta_2}}{\sigma^2_{\beta_1}} + \frac{\sigma^2_{\beta_3}}{A_1^2 \sigma^2_{\beta_1}} \tag{2.49}$$

with

$$\sigma^2_{V_{T1}} = \frac{A^2_{VTn}}{W_1 L_1}, \tag{2.50}$$

$$\sigma^2_{V_{T2}} = \frac{A^2_{VTp}}{W_2 L_2}, \tag{2.51}$$

$$\sigma^2_{V_{T3}} = \frac{A^2_{VTn}}{W_3 L_3}, \tag{2.52}$$

and

$$\sigma_{\beta_1}^2 = \frac{A_{\beta n}^2}{W_1 L_1}, \tag{2.53}$$

$$\sigma_{\beta_2}^2 = \frac{A_{\beta p}^2}{W_2 L_2}, \tag{2.54}$$

$$\sigma_{\beta_3}^2 = \frac{A_{\beta n}^2}{W_3 L_3}. \tag{2.55}$$

Replacing in (2.48) and (2.49) results in

$$\xi_{V_T} = 2\left(\frac{G_{m2}}{G_{m1}}\right)^2 \cdot \left(\frac{A_{VTp}}{A_{VTn}}\right)^2 \cdot \frac{W_1 L_1}{W_2 L_2} + \left(\frac{G_{m3}}{A_1\, G_{m1}}\right)^2 \cdot \frac{W_1 L_1}{W_3 L_3} \tag{2.56}$$

and

$$\xi_{\beta} = 2\left(\frac{A_{\beta p}}{A_{\beta n}}\right)^2 \cdot \frac{W_1 L_1}{W_2 L_2} + \frac{1}{A_1^2}\,\frac{W_1 L_1}{W_3 L_3} \tag{2.57}$$

Similarly to the flicker noise, the input-referred offset (variance or standard deviation) can be reduced by increasing the differential pair $\mathrm{M_{1a}}$-$\mathrm{M_{1b}}$ area $W_1 L_1$ but at the same time also increasing the area of the current mirrors $W_2 L_2$ (and hence $W_{2c} L_{2c}$ and $W_{2d} L_{2d}$) and depending on A_1 also the area of the current mirror $\mathrm{M_{3a}}$-$\mathrm{M_{3b}}$ $W_{3a} L_{3a}$ and $W_{3b} L_{3b}$. This obviously comes at the cost of increased parasitic capacitances at nodes 2, 3 and 4 that will unavoidably reduce the phase margin.

Having done the small-signal, noise and offset analysis, we can now proceed with the design.

3 Design

3.1 Specifications

The OTA specifications are given in Table 3.1.

> **Note**
>
> The specifications given in Table 3.1 are simplified specifications. They are mainly targeting the achievement of a certain gain-bandwidth product GBW and DC gain at lowest current consumption. The GBW sets the differential pair transconductance while the DC gain sets the output conductance. There is an additional specification on the random input-referred offset voltage which, if not met, might eventually require to increase the transistors area. There are no specifications on thermal noise since the transconductance is set by the GBW. There are no specifications on the flicker noise but if the corner frequency was set lower this would required to increase the transistors area. There are also no specifications on the slew-rate, which might be small because of the low-power objective. Finally, there are many more specifications such as CMRR, PSRR, input common-mode voltage range, output-voltage swing, etc... that are not discussed in this example.

Table 3.1: OTA specifications.

Specification	Symbol	Value	Unit
Minimum DC gain	A_{dc}	100	dB
Minimum gain-bandwidth product	GBW	1	MHz
Load capacitance	C_L	1	pF
Maximum input-referred random offset voltage	V_{os}	10	mV
Phase margin	PM	60	$^\circ$

3.2 Process

We will design the cascode gain stage for a generic 180nm bulk CMOS process. The physical parameters are given in Table 3.2, the global process parameters in Table 3.3 and finally the MOSFET parameters in Table 3.4.

Table 3.2: Physical parameters

Parameter	Value	Unit
T	300	K
U_T	25.875	mV

Table 3.3: Global process parameters

Parameter	Value	Unit
V_{DD}	1.8	V
C_{ox}	8.443	$\frac{fF}{\mu m^2}$
W_{min}	200	nm
L_{min}	180	nm

Table 3.4: Transistor process parameters

Parameter	NMOS	PMOS	Unit
sEKV parameters			
n	1.27	1.31	-
$I_{spec\square}$	715	715	nA
V_{T0}	0.455	0.445	V
L_{sat}	26	36	nm
λ	20	20	$\frac{V}{\mu m}$
Overlap capacitances parameters			
C_{GDo}	0.366	0.329	$\frac{fF}{\mu m}$
C_{GSo}	0.366	0.329	$\frac{fF}{\mu m}$
C_{GBo}	0	0	$\frac{fF}{\mu m}$
Junction capacitances parameters			
C_J	1	1.121	$\frac{fF}{\mu m^2}$
C_{JSW}	0.2	0.248	$\frac{fF}{\mu m}$
Flicker noise parameters			
K_F	8.1e-24	8.1e-24	J
AF	1	1	-
ρ	0.05794	0.4828	$\frac{V \cdot m^2}{A \cdot s}$
Matching parameters			
A_{VT}	5	5	$mV \cdot \mu m$
A_β	1	1	$\% \cdot \mu m$
Source and drain sheet resistance parameter			
R_{sh}	600	2386	$\frac{\Omega}{\mu m}$
Width and length parameters			
ΔW	39	54	nm
ΔL	-76	-72	nm

3.3 Design procedure

> **!** Important
>
> For this process, the transistor dimensions are rounded to 10nm. We also will ignore the length and width reduction parameters DL and DW. The main reason is that most of the transistor length and width are sufficiently large that ignoring these parameters has little impact.

We need to start with choosing the curent gain A_3. We have seen that having a current gain $A_3 > 1$ improves the transconductance but at the cost of a higher thermal noise excess factor γ_{ota}. We therefore will set to $A_1 = 1$, $A_2 = 1$ and $A_3 = 1$. Since $A_1 = A_2 = A_3 = 1$, transistors M_{2a}, M_{2b}, M_{2c} and M_{2d} are all identical and so are M_{3a} and M_{3b}. We therefore have the following variables:

- M_{1a}-M_{1b}: W_1, L_1 and I_b. Note that the current I_b is set by G_{m1} because M_{1a}-M_{1b} are biased in weak inversion,
- M_{2a}-M_{2c} and M_{2b}-M_{2d}: IC_2, W_2 and L_2 since the current is already set,
- M_{3a}-M_{3b}: IC_3, W_3 and L_3 since the current is already set,
- M_4: IC_4, W_4 and L_4 since the current is already set,
- M_7: IC_7, W_7 and L_7 since the current is already set,
- M_{5a}-M_{5b}: IC_5, W_5 and L_5 since the current is already set.

We start sizing the differential pair M_{1a}-M_{1b}.

3.3.1 Sizing the differential pair M_{1a}-M_{1b}

In this example there is no specification on the input-referred white noise. Therefore the transconductance G_{m1} is set by the gain-bandwidth product according to

$$GBW = \frac{G_{m1}}{2\pi C_{out}}, \tag{3.1}$$

where G_{m1} is the gate transconductance of M_{1a} and M_{1b} and C_{out} the total output capacitance

$$C_{out} = C_L + C_o \tag{3.2}$$

with C_L the specified load capacitance and C_o the parasitic capacitance at the output node.

In order to minimize the input-referred noise and offset, the input differential pair should be biased in weak inversion. The transconductance G_{m1} in deep weak inversion is then given by

$$G_{m1} = \frac{I_b}{n\,U_T}. \tag{3.3}$$

The bias current I_b is the current flowing in each transistor M_{1a} and M_{1b} when the input differential voltage is zero. The bias current provided by M_{5b} is therefore $2I_b$. The bias current must satisfy the following inequality

$$I_b \geq 2\pi\, n_{0n}\, U_T\, C_L\, GBW_{min}. \tag{3.4}$$

which for the given specifications gives $I_{b,min} = 207\ nA$. The corresponding slew-rate is then equal to $SR_{min} = 207\ mV/\mu s$ which we will consider as sufficient.

> **!** Important
>
> If the slew-rate is not sufficient, the bias current I_b should be increased resulting in a higher current and power consumption. Other options include the use of a class AB OTA [11] or a dynamic/adaptive biasing OTA [12].

As we will see below, the cascode transistors M_4 and M_7 will be biased in weak inversion to save voltage headroom at the output and preserve the output voltage swing of the symmetrical OTA. They will therefore be rather large transistors. Since they are connected to the output, they will increase the parasitic capacitance at the output C_o due mostly to the junction capacitances. To have sufficient margin, we set $I_b = 250\ nA$ and the inversion coefficient to $IC_1 = 0.1$. The transconductance can be calculated from the G_m/I_D function as $G_{m1} = 6.962\ \mu A/V$. Neglecting C_o, this leads to a gain-bandwidth product $GBW = 1.1\ MHz$, which is slightly higher than the target specification offering some margin to account for the additionnal parasitic capacitance C_o. Knowing the drain current I_{D1} and the inversion coefficient, we can calculate the aspect ratio $W_1/L_1 = 3.5$.

Before finalizing the sizing of the differential pair, we first will size the current mirrors.

3.3.2 Sizing the pMOS current mirrors M_{2a}-M_{2c} and M_{2b}-M_{2d}

The gate voltage of M_{2a}-M_{2c} and M_{2a}-M_{2b} should be set as low as possible for a given maximum common mode input voltage $V_{ic,max}$ still keeping M_{1a}-M_{1b} in saturation. The source-to-gate voltage of M_{2a}-M_{2b} V_{SG2} is given by

$$V_{SG2} = V_{DD} - V_{ic,max} + V_{GS1} - V_{DSsat1}. \tag{3.5}$$

The gate-to-source voltage V_{GS1} and the saturation voltage V_{DSsat1} of M_{1a}-M_{1b} are given by $V_{GS1} = 382\ mV$ and $V_{DSsat1} = 105\ mV$. For a maximum input common-mode voltage $V_{ic,max} = 1.3\ V$, the minimum source-to-gate voltage is given by $V_{SG2} = 778\ mV$, corresponding to an inversion coefficient $IC_2 = 21.871$.

We can set V_{SG2} to 800 mV which corresponds to an inversion coefficient $IC_2 = 24.754$ and a saturation voltage $V_{DSsat2} = 277\ mV$. The specific current I_{spec}, aspect ratio and transconductance are then given by $I_{spec2} = 10.10\ nA$, $W_2/L_2 = 0.058$ and $G_{m2} = 1.345\ \mu A/V$.

We now have to make sure that the non-dominant poles f_{p2} and f_{p4} at nodes 2 and 4 are sufficiently higher than the GBW to insure the desired phase margin. The non-dominant pole is given by

$$\omega_{p2} = \frac{G_{m2}}{C_2}, \tag{3.6}$$

where C_2 is the total capacitance at node 2

$$C_2 = 2(C_{GS2} + C_{GB2}). \tag{3.7}$$

Assuming M_{2a}-M_{2b} are in saturation, the gate-to-source capacitance C_{GS2} is given by

$$C_{GS2} \cong W_2\, L_2\, C_{ox} \cdot c_{gsi} + C_{GSop} \cdot W_2, \tag{3.8}$$

where C_{GSop} is the gate-to-source overlap capacitance per unit width for pMOS transistors. c_{gsi} is the intrinsic gate-to-source capacitance normalized to the total gate capacitance $W\, L\, C_{ox}$, which is typically equal to 2/3 in strong inversion and is proportionnal to IC in weak inversion.

The gate-to-bulk capacitance C_{GB2} is given by

$$C_{GB2} \cong\ W_2\, L_2\, C_{ox} \cdot c_{gbi} + C_{GBop} \cdot W_2, \tag{3.9}$$

where C_{GBop} is the gate-to-bulk overlap capacitance per unit width and c_{gbi} is the gate-to-bulk intrinsic capacitance normalized to the total gate capacitance $W\, L\, C_{ox}$ and given by

$$c_{gbi} = \frac{n-1}{n} \cdot c_{gsi}. \tag{3.10}$$

The capacitance at node 2 then scales with W_2 and L_2 according to

$$C_2 = W_2\, L_2 \cdot C_{WL} + W_2 \cdot C_W, \tag{3.11}$$

with

$$C_{WL} = 2\, C_{ox} \cdot (c_{gsi} + c_{gbi}), \tag{3.12}$$

$$C_W = 2(C_{GSop} + G_{GBop}). \tag{3.13}$$

We already have set the inversion coefficient $IC_2 = 24.754$, from which we can calculate $c_{gsi} = 0.595$ and $c_{gbi} = 0.095$. Since the W/L has already been set by the transconductance and the current, we can derive W_2 and L_2 for achieving a given capacitance C_2 according to

$$W_2 = \frac{-C_W \cdot W_2/L_2 + \sqrt{W_2/L_2} \cdot \sqrt{4\, C_2\, C_{WL} + C_W^2 \cdot W_2/L_2}}{2\, C_{WL}}, \tag{3.14}$$

$$L_2 = \frac{W_2}{W_2/L_2}. \tag{3.15}$$

Setting the non-dominant pole f_{p2} to 10 times the GBW, we get $C_2 = 19$ fF, $L_2 = 5.31\ \mu m$ and $W_2 = 310\ nm$.

Since $A_1 = A_3 = 1$, M_{2a}, M_{2b}, M_{2c} and M_{2d} are all identical and hence $W_{2a} = W_{2b} = W_{2c} = W_{2d} = 310\ nm$ and $L_{2a} = L_{2b} = L_{2c} = L_{2d} = 5.31\ \mu m$.

We next size the nMOS current mirror M_{3a} and M_{3b}.

3.3.3 Sizing the nMOS current mirror M_{3a} and M_{3b}

To size M_{3a} and M_{3b} we need to consider the output swing and make sure that M_{2c} remains in saturation for the chosen overdrive voltage chosen for M_{3a}.

Let's start maximizing the output swing assuming that we bias the cascode transistor M_7 in weak inversion for minimum saturation voltage and maximum G_m/I_D. We set the inversion coefficient of M_7 to $IC_7 = 0.1$. The saturation voltage of M_7 is then given by $V_{DSsat7} = 105\ mV$.

Let's say that we want an output swing of 1 V. This means that we have 800 mV to share between the positive and negative saturation voltages which we decide to split equally. This means 400 mV for the saturation voltages of M_7 and M_{3b} which leaves a saturation voltage for M_{3b} of $V_{DSsat3} = 295\ mV$. This corresponds to an inversion coefficient $IC_3 = 28.5$.

We now can check whether with the chosen inversion coefficient for M_{3b}, M_{2c} remains in saturation. The gate-to-source voltage of M_{3a} is $V_{GS3a} = 827\ mV$, giving a source to-drain voltage for M_{2c} $V_{SD2c} = 973\ mV$, which is larger than its saturation voltage $V_{DSsat2c} = 277\ mV$.

Knowing the current and the inversion coefficient $IC_3 = 28.5$, we can deduce $I_{spec3} = 8.759\ nA$, $W_3/L_3 =$ 1.2e-02 and $G_{m3} = 1.261\ \mu A/V$.

Similarly to what was done for transistor M_{2a}-M_{2c}, we need to make sure that the non-dominant pole f_{p3} at node 3 remains much higher than the GBW. Setting $f_{p3}/GBW = 10$ and proceeding in a similar way we get $f_{p3}/GBW = 10$ with $C_3 = 18.1\ fF$ resulting in $W_3 = 140\ nm$ and $L_3 = 11.43\ \mu m$.

We see that W_3 is smaller than the minimum width. If we don't want to increase $W_3\,L_3$ and hence C_3, we need to reduce the inversion coefficient IC_3. We can find the IC such that $W_3 = W_{min}$ for the given f_{p3} by looking at Figure 3.1.

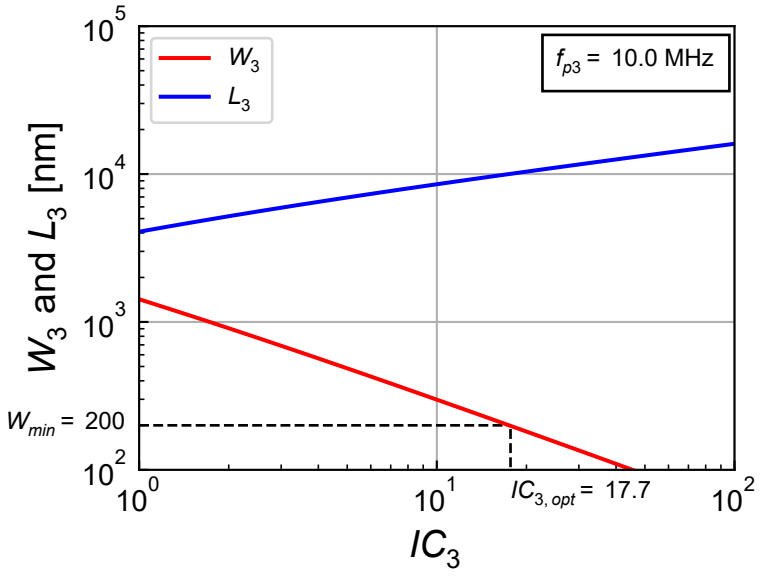

Figure 3.1: Length L_3 and width W_3 of M_3 versus IC_3 for a given f_{p3}/GBW ratio.

We get $IC_3 = 17.7$, $W_3 = 200\ nm$ and $L_3 = 10.11\ \mu m$ with $C_3 = 11.2\ fF$ and $f_{p3}/GBW = 10$.

The inversion coefficient of M_{3a}-M_{3b} is therefore reduced from 28.5 to 17.7 in order to maintain a reasonable parasitic capacitance at node 3 to make sure that f_{p3} is 10-times higher than the GBW.

M_{3b} is identical to M_{3a} and therefore $W_{3a} = W_{3b} = 200\ nm$ and $L_{3a} = L_{3b} = 10.11\ \mu m$.

3.3.4 Sizing the cascode transistors M_4-M_7

The cascode transistors are sized according to the desired DC gain given by

$$A_{dc} = \frac{A_3 \cdot G_{m1}}{G_o} \tag{3.16}$$

where

$$G_o = G_{on} + G_{op} \tag{3.17}$$

with

$$G_{on} = \frac{G_{ds3b} \cdot G_{ds7}}{G_{ms7}} \tag{3.18}$$

$$G_{op} = \frac{G_{ds2d} \cdot G_{ds4}}{G_{ms4}} \tag{3.19}$$

the output conductance of of the nMOS and pMOS cascode stages, respectively. The minimum DC gain specification is given by $A_{dc} = 1.0\text{e+}05$ or $A_{dc} = 100$ dB. Since the transconductance G_{m1} is already set by the GBW, the output conductance at the output node G_o is then given by $G_o = G_{m1}/A_{dc} = 0.070\ nA/V$. We will split the output conductance equally between the nMOS and pMOS cascodes. We already have set the inversion coefficient of M_7 to $IC_7 = 0.1$. Knowing the current, we can deduce the specific current $I_{spec7} = 2.5\ \mu A$ and the aspect ratio $W_7/L_7 = 3.5$. Knowing the current and IC_7 we can get $G_{ms7} = 8.851\ \mu A/V$.

We already have chosen the length of M_{3a}-M_{3b} $L_3 = 10.11\ \mu m$. The output conductance of M_{3b} can then be estimated to $G_{ds3} = 1.236\ nA/V$. We can then deduce the output conductance of M_7 as $G_{ds7} = 249.286\ nA/V$ from which we deduce its length $L_7 = 0.05\ \mu m$ which is smaller than the minimum length.

To have some margin and avoid DIBL, we choose a slightly longer length $L_7 = 360\ nm$. Keeping the same $W_7/L_7 = 3.5$, we get $W_7 = 1.26\ \mu m$.

The minimum value of the bias voltage V_{b2} is set such that M_{3b} remains in saturation

$$V_{b2,min} = V_{DSsat3} + V_{GS2}. \tag{3.20}$$

The saturation voltage of M_{3b} is equal to $V_{DSsat3} = 241\ mV$ and the V_{GS} voltage of M_7 is $V_{GS7} \cong 455\ mV$, which results $V_{b2,min} = 696\ mV$. For convenience we choose $V_{b2} = V_{DD}/2 = 900\ mV$.

For M_4 we set the same inversion coefficient as M_7 $IC_4 = IC_7 = 0.1$, from which we get its saturation voltage $V_{DSsat4} = 105\ mV$. Knowing the current and the IC we can deduce $I_{spec4} = 2.5\ \mu A$ and $W_4/L_4 = 14.4$. The source transconductance of M_4 is then given by $G_{ms4} = 8.851\ \mu A/V$. The output conductance of M_{2d} can be estimated as $G_{ds2} = 2.354\ nA/V$. We can then deduce the output conductance of M_4 as $G_{ds4} = 130.880\ nA/V$, from which we can calculate the length $L_4 = 100\ nm$, which is smaller than the minimum length.

We could choose $L_4 = L_{min}$, but in order to have some margin on the DC gain, we choose $L_4 = 250\ nm$. Keeping the same $W_4/L_4 = 14.4$, this leads to $W_4 = 3.61\ \mu m$.

The maximum value of the bias voltage V_{b1} is limited by the saturation voltage of M_{2d} according to

$$V_{b1,max} = V_{DD} - V_{SDsat2d} - V_{SG4}. \tag{3.21}$$

The saturation voltage of M_{2d} is $V_{SDsat2} = 277\ mV$ and the source-to-gate voltage of M_4 is $V_{SG4} \cong 445\ mV$, leading to $V_{b1,max} \cong 1.078\ V$. For convenience, we can also set $V_{b1} = V_{DD}/2 = 900\ mV$.

We can now check the resulting DC gain. The output conductance of the nMOS and pMOS cascodes are $G_{on} = 4.848\ pA/V$ and $G_{op} = 13.298\ pA/V$, respectively. This results in a total output conductance $G_o = 18.146\ pA/V$ and a DC gain $A_{dc} = 4e{+}05$ or $A_{dc} = 111.7$ dB, which is 11.7 dB higher than the specifications.

3.3.5 Sizing the nMOS current mirror M_{5a}-M_{5b}

Finally we need to size M_{5a}-M_{5b}. The minimum input common mode voltage $V_{ic,min}$ is limited by the saturation voltage of M_{5b} according to

$$V_{ic,min} = V_{GS1} + V_{DSsat5b}. \tag{3.22}$$

Since M_{1a}-M_{1b} are in a separate well, their gate-to-source voltage is $V_{GS1} = V_{T0n} + n\,U_T\,(v_p - v_s) \cong 382\ mV$. Setting the minimum input common mode voltage to $V_{ic,min} = 600\ mV$ leads to the maximum saturation voltage of M_{5b} $V_{DSsat5} = V_{ic,min} - V_{GS1} \cong 218\ mV$. The corresponding inversion coefficient of M_{5b} is $IC_5 = 13.7$. From I_b and IC_5 we get $I_{spec5} = 36.547\ nA$ and $W_5/L_5 = 5.111e{-}02$. With such a low W/L ratio, we need to set W_5 to the minimum width $W_5 = W_{min} = 200\ nm$ from which we deduce $L_5 = 3.91\ \mu m$.

Transistor M_{5a} is identical to M_{5b} and hence $W_{5a} = W_{5b} = 200\ nm$ and $L_{5a} = L_{5b} = 3.91\ \mu m$.

The sizing process is almost finished, but we still need to finalize the sizing of the differential pair M_{1a}-M_{1b}.

3.3.6 Final sizing of the differential pair M_{1a}-M_{1b}

We haven't finalized the sizing of M_{1a}-M_{1b}. We already have the W/L ratio but still need to set W_1 and L_1. We don't have any specifications on the noise and particularly the corner frequency, while the white noise is already set by the transconductance G_{m1}.

Since the current mirrors current gains are all unity $A_1 = A_2 = A_3 = 1$, the transistors M_{2a}, M_{2b}, M_{2c} and M_{2d} are all identical. In this case the contributions of the current mirrors to the input-referred flicker noise relative to the contribution of the differential pair is captured by the η_{fl} parameter recalled below

$$\eta_{fl} = 2\,\frac{\rho_p}{\rho_n} \cdot \left(\frac{G_{m2}}{G_{m1}}\right)^2 \frac{W_1 L_1}{W_2 L_2} + \left(\frac{G_{m3}}{G_{m1}}\right)^2 \cdot \frac{W_1 L_1}{W_3 L_3}. \tag{3.23}$$

The ratio of the flicker noise parameter of pMOS transistors to that of nMOS transistors is given by $\rho_p/\rho_n = 8.333$, which is rather large. The square of the transconductance ratio $(G_{m1}/G_{m2})^2 = 26.793$ should compensate for this large ρ_p/ρ_n ratio. We can try to make the contribution of the input differential pair equal to the contribution of the current mirrors (i.e. set $\eta_{fl} = 1$). This results in $W_1 \cdot L_1 = 2.474\ \mu m^2$.

Since we already have W_1/L_1 we can deduce $W_1 = 2.94\ \mu m$ and $L_1 = 840\ nm$. Since transistor M_{1a} is identical to M_{1b}, we have $W_{1a} = W_{1b} = 2.94\ \mu m$ and $L_{1a} = L_{1b} = 840\ nm$.

The relative contribution to the input-referred flicker noise of the pMOS current mirrors M_{2a} to M_{2d} is 0.933, whereas that of the nMOS current mirror M_{3a} and M_{3b} is 0.065. This leads to $\eta_{fl} = 0.998$, which is close to the desired $\eta_{fl} \cong 1$.

We now have finalized the design. We can still check the thermal noise. The contributions of the current mirrors to the input-referred white noise relative to that of the differential pair is $\eta_{th} = 0.775$. This results in an OTA thermal noise excess factor $\gamma_{ota} = 2.3$. The input-referred white noise resistance

is $R_{ninth} = 333.2\ k\Omega$, corresponding to a PSD S_{ninth} = 5.5e-15 V^2/Hz or $\sqrt{S_{ninth}} = 74.3\ nV/\sqrt{Hz}$ or $10 \cdot \log(S_{ninth})$ = -142.6 $dBv/\sqrt{Hz}$. This sets the corner frequency to $f_k = 281.4\ kHz$.

The design is now finalized and is summarized in the section.

3.4 Summary

3.4.1 Specifications

The specifications are recalled in Table 3.5.

Table 3.5: OTA specifications.

Specification	Symbol	Value	Unit
Minimum DC gain	A_{dc}	100	dB
Minimum gain-bandwidth product	GBW	1	MHz
Load capacitance	C_L	1	pF
Maximum input-referred random offset voltage	V_{os}	10	mV
Phase margin	PM	60	$^\circ$

3.4.2 Bias

The bias information are summarized in Table 3.6.

Table 3.6: OTA bias.

Bias voltage or current	Symbol	Value	Unit
Supply voltage	V_{DD}	1.8	V
Bias current	I_b	250.0	nA
Cascode bias voltage	V_{b1}	0.9	V
Cascode bias voltage	V_{b2}	0.9	V

3.4.3 Transistor information

The transistor sizes and large-signal variables are summarized in Table 3.7, whereas Table 3.8 gives the small-signal and thermal noise parameters. An Excel table is generated with more information (e.g. all the parasitic capacitances).

Table 3.7: Transistor size and bias information.

Transistor	$W\ [\mu m]$	$L\ [\mu m]$	$I_D\ [nA]$	$I_{spec}\ [nA]$	IC	$V_G - V_{T0}\ [mV]$	$V_{DSsat}\ [mV]$
M1a	2.94	0.84	250	2503	0.1	-45	105
M1b	2.94	0.84	250	2503	0.1	-45	105
M2a	0.31	5.31	250	10	24.7	208	277
M2b	0.31	5.31	250	10	24.7	208	277
M2c	0.31	5.31	250	10	24.7	208	277
M2d	0.31	5.31	250	10	24.7	208	277
M3a	0.20	10.11	250	14	17.7	179	241
M3b	0.20	10.11	250	14	17.7	179	241
M4	3.61	0.25	250	2500	0.1	-44	105

Table 3.7: Transistor size and bias information.

Transistor	$W\ [\mu m]$	$L\ [\mu m]$	$I_D\ [nA]$	$I_{spec}\ [nA]$	IC	$V_G - V_{T0}\ [mV]$	$V_{DSsat}\ [mV]$
M5a	0.20	3.91	500	37	13.7	155	218
M5b	0.20	3.91	500	37	13.7	155	218
M7	1.26	0.36	250	2503	0.1	-45	105

Table 3.8: Transistor small-signal and thermal noise parameters.

Transistor	$G_{spec}\ [\mu A/V]$	$G_{ms}\ [\mu A/V]$	$G_m\ [\mu A/V]$	$G_{ds}\ [nA/V]$	γ_n
M1a	96.716	8.852	6.962	14.881	0.653
M1b	96.716	8.852	6.962	14.881	0.653
M2a	0.391	1.757	1.345	2.354	0.831
M2b	0.391	1.757	1.345	2.354	0.831
M2c	0.391	1.757	1.345	2.354	0.831
M2d	0.391	1.757	1.345	2.354	0.831
M3a	0.546	2.041	1.605	1.236	0.803
M3b	0.546	2.041	1.605	1.236	0.803
M4	96.620	8.851	6.777	50.000	0.671
M5a	1.413	4.567	3.592	6.394	0.797
M5b	1.413	4.567	3.592	6.394	0.797
M7	96.716	8.852	6.962	34.722	0.653

4 OTA Characteristics

In this section, we check whether the specs are achieved.

4.1 Open-loop gain

We can calculate the various OTA features related to the open-loop transfer function, which are given in Table 4.1.

Table 4.1: OTA gain variables.

Symbol	Theoretical Value	Unit
A_{dc}	112	dB
G_{m1}	6.962	$\mu A/V$
G_{m2}	1.345	$\mu A/V$
G_{m3}	1.605	$\mu A/V$
f_0	2.872	Hz
GBW	1.102	MHz
f_{p2}	11.049	MHz
f_{p3}	11.08	MHz
f_{p4}	11.049	MHz

The gain-bandwidth product from the specifications is repeated here

$GBW = 1.000$ MHz (from spec).

The estimated value assuming that all the non-dominant poles are much higher than the GBW is given by

$GBW_{est} = 1.102$ MHz (estimation).

The GBW accounting for the effect of the additional non-dominant poles is given by

$GBW_{the} = 1.093$ MHz (theory).

We see that there is only a small difference between GBW_{est} and GBW_{the}, which confirms that the non-dominant poles are sufficiently far from GBW as stated in Table 4.1.

We can now plot the gain response using the variables given in Table 4.1. It is shown in Figure 4.1.

4.2 Input-referred noise

We can now compute all the parameters needed for the calculation of the OTA thermal noise excess factor and its input-referred thermal noise PSD and resistance. They are given in Table 4.2.

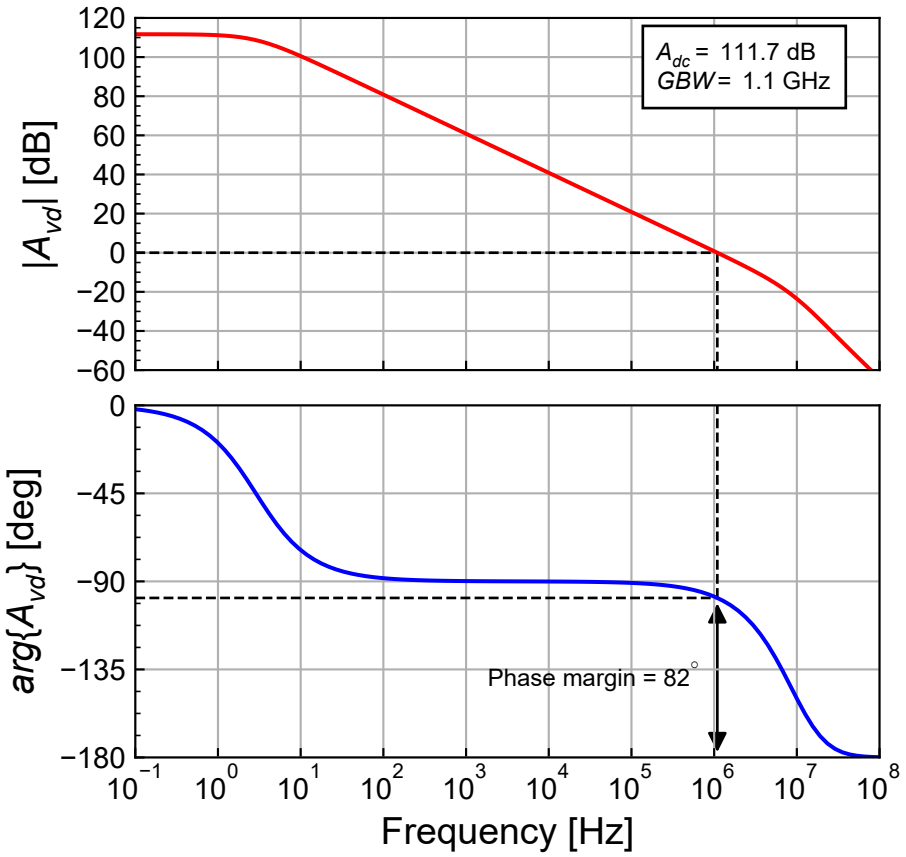

Figure 4.1: OTA theoretical transfer function.

Table 4.2: OTA thermal noise parameters.

Symbol	Theoretical Value	Unit
G_{m1}	6.962	$\mu A/V$
G_{m2}	1.345	$\mu A/V$
G_{m3}	1.605	$\mu A/V$
G_{m1}/G_{m2}	5.175	-
G_{m1}/G_{m3}	4.338	-
γ_{n1}	0.653	-
γ_{n2}	0.831	-
γ_{n3}	0.803	-
η_{th}	0.775	-
γ_{ota}	2.319	-
R_{nt}	333.146	$k\Omega$
S_{ninth}	5.5e-15	V^2/Hz
$\sqrt{S_{ninth}}$	74.276	$nV/\sqrt{Hz}$
$10 \cdot \log(S_{ninth})$	-142.583	$dBv/\sqrt{Hz}$

From the value of $\eta_{th} = 0.775$ in Table 4.2, we see that the current mirrors M_{2a}-M_{2b}-M_{2c}-M_{2d} and M_{3a}-M_{3b} contribute about equally to the OTA input-referred thermal noise PSD. The OTA thermal noise excess factor is therefore about twice that of the differential pair $2\,\gamma_{n1}$.

We can now compute all the parameters needed for the calculation of the input-referred flicker noise and the corner frequency. They are given in Table 4.3.

Table 4.3: OTA flicker noise parameters.

Symbol	Theoretical Value	Unit
$(G_{m1}/G_{m2})^2$	26.8	-
$(G_{m1}/G_{m3})^2$	18.8	-
ρ_p/ρ_n	8.3	-
$\frac{W_1 \cdot L_1}{W_2 \cdot L_2}$	1.2	-
$\frac{W_1 \cdot L_1}{W_3 \cdot L_3}$	0.9	-
η_{fl}	0.793	-
$\sqrt{S_{ninfl}(1\,Hz)}$	38.9	$\mu V/\sqrt{Hz}$
$10 \cdot \log(S_{ninfl}(1\,Hz))$	-88.2	$dBv/\sqrt{Hz}$
f_k	274.1	kHz

Similarly to thermal noise, from the value of $\eta_{fl} = 0.793$ in Table 4.3, we see that the current mirrors M_{2a}-M_{2b}-M_{2c}-M_{2d} and M_{3a}-M_{3b} contribute about equally to the OTA input-referred flicker noise PSD, despite the large $\rho_p/\rho_n = 8.333$ ratio and the smaller area of the current mirrors compared to the differential pair. This is achieved because of the high gains $(G_{m1}/G_{m2})^2 = 26.8$ and $(G_{m1}/G_{m3})^2 = 18.8$.

We can plot the input-referred noise PSD which is shown in Figure 4.2. The corner frequency is estimated at $f_k = 274.1\ kHz$.

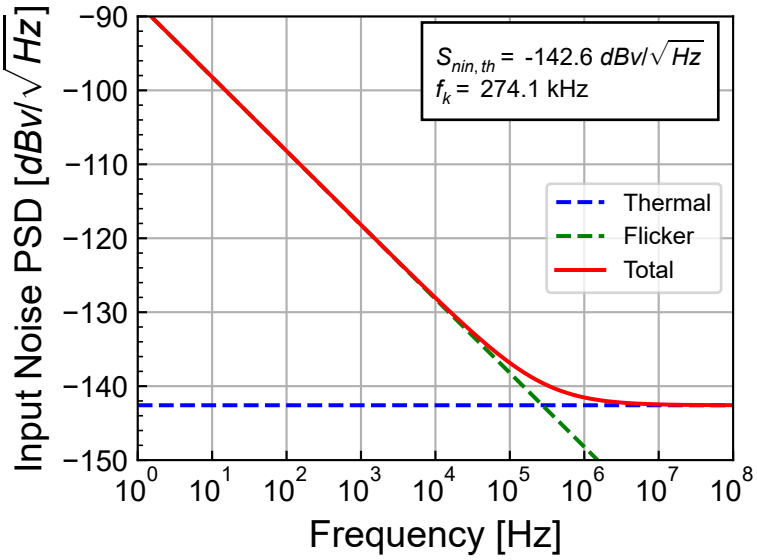

Figure 4.2: OTA theoretical input-referred noise PSD.

4.3 Input-referred offset voltage

The variance of the input-referred offset for $A_1 = A_2 = A_3 = 1$ is given by (2.47) which can be rewritten as

$$\sigma^2_{V_{os}} = \sigma^2_{V_T} + \sigma^2_{\beta} \tag{4.1}$$

where

$$\sigma^2_{V_T} = \sigma^2_{V_{T1}} \cdot (1 + \xi_{V_T}) \tag{4.2}$$

and

$$\sigma^2_{\beta} = \left(\frac{I_b}{G_{m1}}\right)^2 \cdot \sigma^2_{\beta_1} \cdot (1 + \xi_{\beta}). \tag{4.3}$$

ξ_{V_T} represents the V_T-mismatch contributions to the input-referred offset of the current mirrors relative to that of the differential pair. It is given by (2.56) which is repeated here

$$\xi_{V_T} = 2\left(\frac{G_{m2}}{A_1\, G_{m1}}\right)^2 \cdot \left(\frac{A_{VTp}}{A_{VTn}}\right)^2 \cdot \frac{W_1 L_1}{W_2 L_2} + \left(\frac{G_{m3}}{G_{m1}}\right)^2 \cdot \frac{W_1 L_1}{W_3 L_3} \tag{4.4}$$

and ξ_β represents the β-mismatch contributions to the input-referred offset of the current mirrors relative to that of the differential pair. It is given by (2.57) which is repeated below

$$\xi_\beta = 2\left(\frac{A_{\beta p}}{A_{\beta n}}\right)^2 \cdot \frac{W_1 L_1}{W_2 L_2} + \frac{1}{A_1^2} \cdot \frac{W_1 L_1}{W_3 L_3}. \tag{4.5}$$

with

$$\sigma^2_{V_{T1}} = \frac{A^2_{VTn}}{W_1 L_1}, \tag{4.6}$$

$$\sigma^2_{V_{T2}} = \frac{A^2_{VTp}}{W_2 L_2}, \tag{4.7}$$

$$\sigma^2_{V_{T3}} = \frac{A^2_{VTn}}{W_3 L_3}, \tag{4.8}$$

and

$$\sigma^2_{\beta 1} = \frac{A^2_{\beta n}}{W_1 L_1}, \tag{4.9}$$

$$\sigma^2_{\beta 2} = \frac{A^2_{\beta p}}{W_2 L_2}, \tag{4.10}$$

$$\sigma^2_{\beta 3} = \frac{A^2_{\beta n}}{W_3 L_3}. \tag{4.11}$$

The parameter for calculating the standard deviation of the input-referred offset voltage are given in Table 4.4.

Table 4.4: OTA input-referred offset parameters.

Symbol	Theoretical Value	Unit
σ_{VT1}	3.182	mV
σ_{VT2}	3.897	mV
σ_{VT3}	3.516	mV
$\sigma_{\beta 1}$	0.6	%
$\sigma_{\beta 2}$	0.8	%
$\sigma_{\beta 3}$	0.7	%
ξ_{VT}	0.177	-
ξ_β	4.221	-
σ^2_{VT}	11.914	mV^2
σ_{VT}	3.452	mV
σ^2_β	0.3	mV^2
σ_β	0.5	mV
σ_{Vos}	3.491	mV

From Table 4.4, we see that the β-mismatch is negligible and that the input-referred offset voltage is dominated by the contribution of the V_T-mismatch from the differential pair.

4.4 Current and power consumption

The total current consumption, ignoring the current drawn by M_{5a}, is $I_{tot} = (2 + A_1 + A_3) \cdot I_b$. Assuming the input differential pait M_{1a}-M_{1b} is biased in weak inversion, the bias current is directly related to the gain-bandwidth product GBW according to

$$I_b \cong nU_T \cdot \frac{C_L}{A_3} \cdot GBW. \tag{4.12}$$

The minimum total current consumption can then be estimated as

$$I_{tot,min} \cong \frac{2 + A_1 + A_3}{A_3} \cdot nU_T \cdot C_L \cdot GBW. \tag{4.13}$$

The bias current and the total current are proportional to the gain-bandwidth product GBW and the load capacitance C_L. In the case $A_1 = A_2 = A_3 = 1$, we have

$I_{tot,min} \cong 4 \cdot nU_T \cdot C_L \cdot GBW = 827\ nA.$

The actual current consumption accounting for some margin taken on the GBW is given by

$I_{tot} = 4I_b = 1.00\ \mu A$ which is 1.210 larger than the absolute minimum current consumption. This larger current consumption is mostly due to the parasitic capacitances at the output which add to the exsiting load capacitance and require a larger transconductance and hence a larger current to achive the same GBW.

The above design will now be checked against simulations.

5 Simulation results from ngspice

The theoretical results can be validated with the results obtained from simulations performed with ngspice. In order to run the simulations you need to have ngspice correctly installed. Please refer to the installation instructions.

> **Note**
>
> The simulations are performed with ngspice [5] using the EKV 2.6 compact model [6] [13] [2]. For ngspice, we use the original Verilog-A implementation of EKV 2.6 [8] modified by C. Enz to get the operating point informations and available on the Gitub va-models site provided by D. Warning at [7] [14]. The Verilog-A code was then compiled with OpenVAF [15] to generate the OSDI for running it with ngspice. The parameters correspond to a generic 180 nm bulk CMOS process [9].

5.1 Operating point

We first write the parameter file for this specific design for running the ngspice simulations. Before running the AC and NOISE simulations, we first need to check the quiescent voltages and currents and the operating points of all transistors by running a .OP simulation.

Table 5.1: OTA node voltages with the OTA in open-loop without offset correction.

Node	Voltage
vdd	1.8
vb1	0.9
vb2	0.9
inp	0.9
inn	0.9
out	0.318007
ic	0.9
id	0
1	0.490628
2	0.993525
3	0.728736
4	0.993525
5	0.313181
6	1.41383
8	0.69466

From the node voltages shown in Table 5.1, we see that the output voltage $V_{outq} = 318\ mV$ is too low and is pushing M_7 and M_{3b} out of saturation. This is due to the current mismatch in M_{2c} and M_{2d} and between M_{3a} and M_{3b} due to different drain voltages and finite output conductances leading to a different current flowing in M_{2d} and M_4 compared to that flowing in M_{3b} and M_7. Even if the current

difference is very small, it results in a large voltage debiasing at the output because of the high output resistance provided by the cascode stages.

Therefore simulating the open-loop gain for high gain amplifiers is not easy to perform without closing the loop. There are basically two approaches to simulate the open-loop gain for high-gain amplifiers:

1) Imposing a DC offset voltage to the amplifier in open-loop configuration that brings the output voltage back to the high gain region (for example equal to the input common-mode voltage) or
2) Simulating the closed-loop gain (for example in voltage follower mode with a feedback gain of 1 and extracting the open-loop gain from the closed loop gain according to

$$A_{open\text{-}loop}(\omega) = \frac{A_{closed\text{-}loop}(\omega)}{1 - A_{closed\text{-}loop}(\omega)}, \tag{5.1}$$

where $A_{closed\text{-}loop}(\omega)$ is the simulated closed-loop transfer function and $A_{open\text{-}loop}(\omega)$, the computed open-loop transfer function. The above relation assumes that the open-loop DC gain is large enough for the input-referred offset voltage to be ignored.

The input-referred offset voltage can be extracted from the closed-loop voltage follower circuit as

$$V_{os} = V_{in} - \left(1 + \frac{1}{A}\right) \cdot V_{out} \cong V_{in} - V_{out} \quad \text{for } A \gg 1, \tag{5.2}$$

where $A \triangleq A_{open\text{-}loop}(0)$ is the open-loop DC gain which can be assumed to be much larger than 1. This means that, provided the DC open-loop gain is sufficiently large, the offset voltage can be measured at the amplifier differential input after imposing the proper input common-mode voltage V_{ic}.

We can now simulate the OTA in closed-loop as a voltage follower.

Table 5.2: OTA node voltages with the OTA in voltage follower configuration.

Node	Voltage
vdd	1.8
vb1	0.9
vb2	0.9
inp	0.9
out	0.899926
1	0.490592
2	0.993722
3	0.728579
4	0.993329
5	0.385322
6	1.41676
8	0.69466

From the node voltages of the OTA in voltage follower configuration shown in Table 5.2, we see that now the quiescent ouput voltage $V_{outq} = 900\ mV$ is very close to the input voltage that has been set to $V_{ic} = 900\ mV$. We can then extract the corresponding offset voltage $V_{os} \cong V_{in} - V_{out} = 74.000\ \mu V$.

We can now apply this offset voltage to the open-loop operating point point simulation.

Table 5.3: OTA node voltages with the OTA in open-loop including offset correction.

Node	Voltage
vdd	1.8

Table 5.3: OTA node voltages with the OTA in open-loop including offset correction.

Node	Voltage
vb1	0.9
vb2	0.9
inp	0.900037
inn	0.899963
out	0.932997
ic	0.9
id	7.4e-05
1	0.490628
2	0.993722
3	0.728579
4	0.993329
5	0.385506
6	1.41694
8	0.69466

From the node voltages of the OTA in open-loop configuration shown in Table 5.3 after adding the offset voltage at the input, we see that now the quiescent ouput voltage $V_{outq} = 933\ mV$ of the open-loop circuit is sufficiently close to the common-mode input voltage $V_{ic} = 900\ mV$.

The operating point information for all transistors coming from the EKV2.6 compact model are extracted from the ngspice .op.dat file. The data is split into the large-signal operating informations presented in Table 5.4, the small-signal operating point informations shown in Table 5.5 and the noise operating point informations in Table 5.6.

We can compare the results of the .op file (for example the inversion coefficient IC) to the results of the design given in Table 3.7. We observe that the values are close.

Similarly we can compare the small-signal parameters (for example the gate transconductance G_m) resulting from the .op file to the results of the design presented in Table 3.8. Again, we see that they are reasonably close.

Table 5.4: Operating point information extracted from ngspice .op file for each transistor.

Transistor	$I_D\ [nA]$	$I_{spec}\ [nA]$	IC [-]	n [-]	$V_{DSsat}\ [mV]$
M1a	249.3	2855.9	0.087	1.27	119
M1b	249.8	2855.8	0.088	1.27	119
M2a	249.3	10.2	24.527	1.31	360
M2b	249.8	10.2	24.580	1.31	360
M2c	249.5	10.2	24.531	1.31	360
M2d	249.2	10.2	24.574	1.31	360
M3a	249.5	15.2	16.403	1.27	313
M3b	249.2	15.2	16.399	1.27	313
M4	249.2	3202.5	0.078	1.31	118
M5a	500.0	40.2	12.465	1.27	286
M5b	499.1	40.2	12.459	1.27	286
M7	249.2	3124.7	0.080	1.27	118

Table 5.5: Small-signal operating point information extracted from ngspice .op file for each transistor.

Transistor	G_m $[\mu A/V]$	G_{ms} $[\mu A/V]$	G_{ds} $[nA/V]$
M1a	6.887	8.892	17.199
M1b	6.899	8.908	17.239
M2a	1.282	1.736	0.977
M2b	1.283	1.737	0.979
M2c	1.283	1.737	0.872
M2d	1.276	1.734	6.448
M3a	1.601	2.063	0.718
M3b	1.598	2.060	2.213
M4	7.045	8.976	49.487
M5a	3.617	4.658	3.899
M5b	3.610	4.650	5.156
M7	7.215	8.902	48.158

Table 5.6: Noise operating point information extracted from ngspice .op file for each transistor.

Transistor	R_n $[k\Omega]$	$\sqrt{S_{ID,th}}$ $[nA/\sqrt{Hz}]$	γ_n [-]	$\sqrt{S_{ID,fl}}$ at 1Hz $[nA/\sqrt{Hz}]$
M1a	97.498	40.201	0.671	20510.5
M1b	97.319	40.164	0.671	20510.5
M2a	689.211	106.885	0.883	64689.4
M2b	688.582	106.836	0.883	64689.4
M2c	688.506	106.830	0.883	64689.4
M2d	694.707	107.310	0.887	64689.4
M3a	522.597	93.073	0.837	19981.2
M3b	523.954	93.194	0.837	19981.2
M4	93.364	39.340	0.658	110606
M5a	229.943	61.738	0.832	32324.5
M5b	230.419	61.802	0.832	32324.5
M7	88.846	38.376	0.641	50944.1

We can also check the bias voltages and operating region of each transistor which are given in Table 5.7.

Table 5.7: Bias voltages and operating regions extracted from ngspice for each transistor.

Trans.	Type	Funct.	V_G $[V]$	V_S $[V]$	V_D $[V]$	V_{DS} $[mV]$	V_{DSsat} $[mV]$	Reg.	Sat.
M1a	n	DP	0.409	0.000	0.503	503	119	WI	sat
M1b	n	DP	0.409	0.000	0.503	503	119	WI	sat
M2a	p	CM	0.806	0.000	0.806	806	360	SI	sat
M2b	p	CM	0.807	0.000	0.807	807	360	SI	sat
M2c	p	CM	0.806	0.000	1.071	1071	360	SI	sat
M2d	p	CM	0.383	0.000	0.383	383	360	SI	sat
M3a	n	CM	0.729	0.000	0.729	729	313	SI	sat
M3b	n	CM	0.729	0.000	0.386	386	313	SI	sat
M4	p	CA	0.900	0.383	0.867	484	118	WI	sat
M5a	n	CM	0.695	0.000	0.695	695	286	SI	sat
M5b	n	CM	0.695	0.000	0.491	491	286	SI	sat
M7	p	CA	0.900	0.386	0.933	547	118	WI	sat

From Table 5.4, we see that all transistors have a sufficiently large V_{DS} voltage and are therefore biased in saturation. Additionnally we see that all the saturation voltages in the output current branch M_{2d}, M_4, M_7 and M_{3b} are summing up to 909 mV leaving an output voltage swing about equal to $V_{out,swing} \cong 891\ mV$. This output voltage swing could be increased by about 250 mV by biasing M_{2d} and M_{3b} in weak inversion. This would be at the cost of larger transistors and a less current matching in the current mirrors.

From Table 5.7, we see that all transistors are biased in saturation. The operating points look fine. We can now proceed with the simulation of the open-loop large-signal transfer characteristic.

5.2 Large-signal differential transfer characteristic

We now simulate the DC differential transfer characteristic. We can then check the systematic offset voltage that was extracted above. The simulation of the large-signal input-output characteristic is presented in Figure 5.1.

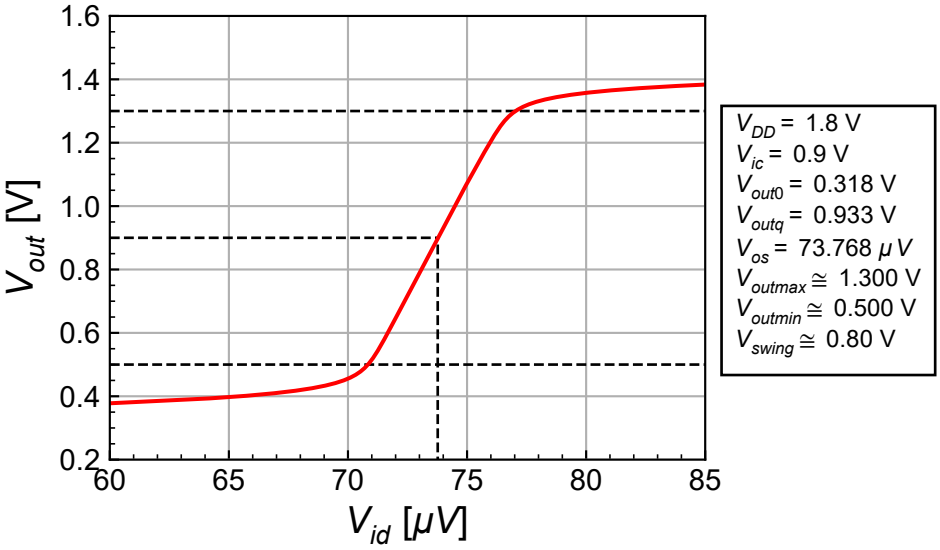

Figure 5.1: Simulated large-signal input-output characteristic.

From Figure 5.1, we see that the output swing is about $V_{out,swing} \cong 800\ mV$, which is slightly less than the above estimation. We can now zoom into the high gain region in order to extract the offset voltage that is needed to bring the output voltage back to $V_{outq} = V_{ic} = 0.900\ V$. The simulation results are presented in Figure 5.2.

We can now save a more accurate value of the offset voltage $V_{os} = 73.768\ \mu V$ that is required to bring the output voltage to $V_{ic} = 900\ mV$ and that will be used for the following .AC and .NOISE simulations.

5.3 Open-loop gain

5.3.1 Closed-loop circuit

As explained above we can extract the open-loop gain from the simulated closed-loop gain with the amplifier operating as a voltage follower. The open-loop gain is then given by

$$A_{open\text{-}loop}(\omega) = \frac{A_{closed\text{-}loop}(\omega)}{1 - A_{closed\text{-}loop}(\omega)}, \tag{5.3}$$

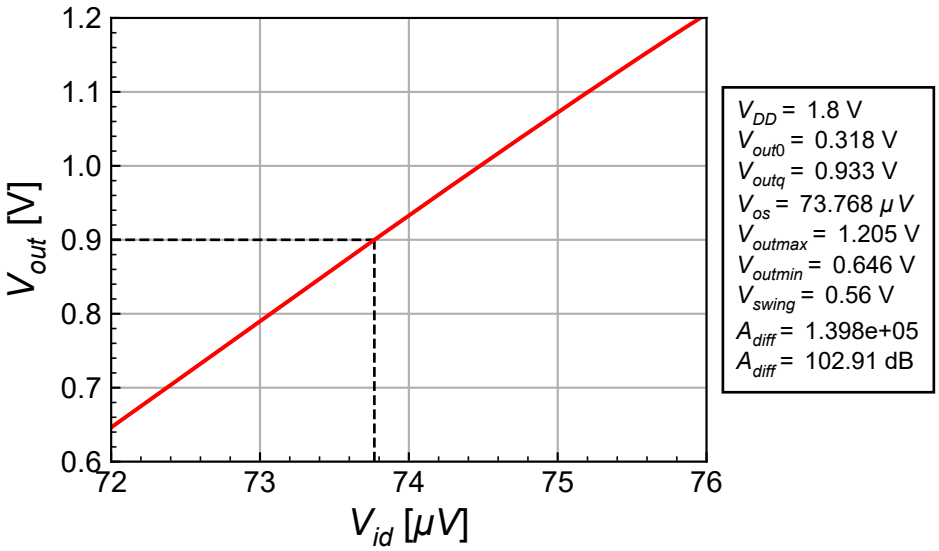

Figure 5.2: Zoom of the simulated large-signal input-output characteristic in the gain region.

where $A_{closed\text{-}loop}(\omega)$ is the simulated closed-loop transfer function and $A_{open\text{-}loop}(\omega)$, the computed open-loop transfer function. The above relation assumes that the open-loop DC gain is large enough for the input-referred offset voltage to be ignored.

Note that we need to have a sufficient number of digits for the simulated closed-loop gain because the latter is very close to 1. The simulations results are shown in Figure 5.3.

From Figure 5.3, we see that the simulated GBW is right on target but slightly smaller than the estimated value. The simulated DC gain is much smaller than the theoretical estimation but slightly above spec. We can now simulate the open-loop gain directly in open-loop configuration and compare the results to those achieved from the closed-loop simulation.

5.3.2 Open-loop circuit

After having checked the operating point information, extracted the offset voltage and making sure that the OTA output is not saturated, we can now proceed with the open-loop gain simulation. The simulation results are presented in Figure 5.4.

The results of the open-loop simulation in Figure 5.4 are very close to the result extracted from the closed-loop simulation except at high frequency (above the GBW frequency). The GBW is the same than the value extracted from the closed-loop simulation, smaller than the estimated one but still on target. The DC gain obtained from the open-loop simulation gain is slightly smaller than the value extracted from the closed-loop simulation and much smaller than the theoretical estimation, but still within spec. The low value of the DC gain is due to the high output conductance of nMOS transitors in this technology, while the difference between simulation and theoretical prediction is due to the poor output conductance model that is used in the design phase.

5.4 Input-referred noise

The simulated input-referred noise PSD is presented in Figure 5.5 and compared to the theoretical estimation.

From Figure 5.5, we see a perfect match between simulation and theoretical estimation for both the flicker noise and the white noise except aˆbove the GBW where the simulated noise PSD becomes

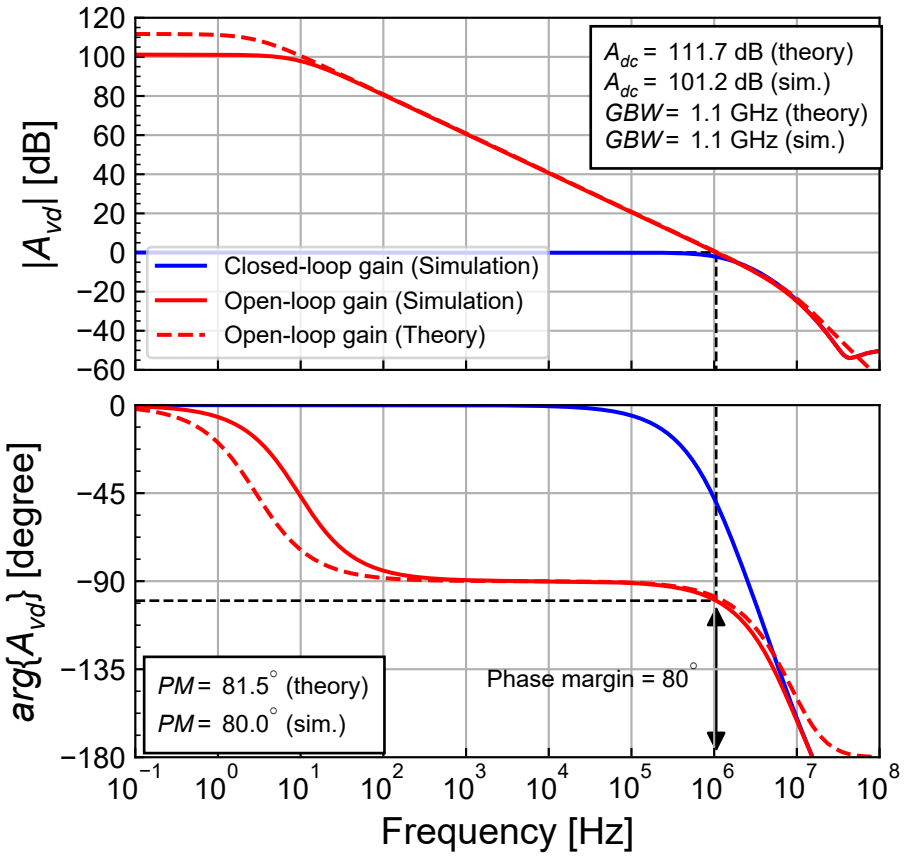

Figure 5.3: Open-loop gain response extracted from the closed-loop simulations and compared to theoretical estimation.

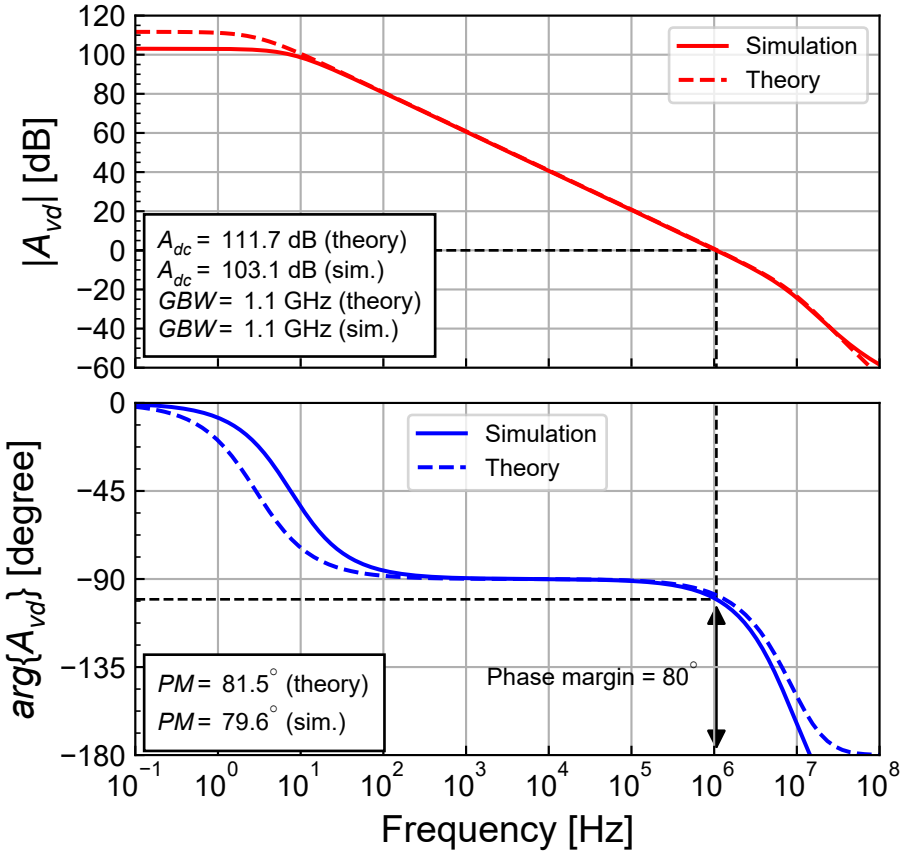

Figure 5.4: Simulated gain response compared to theoretical estimation.

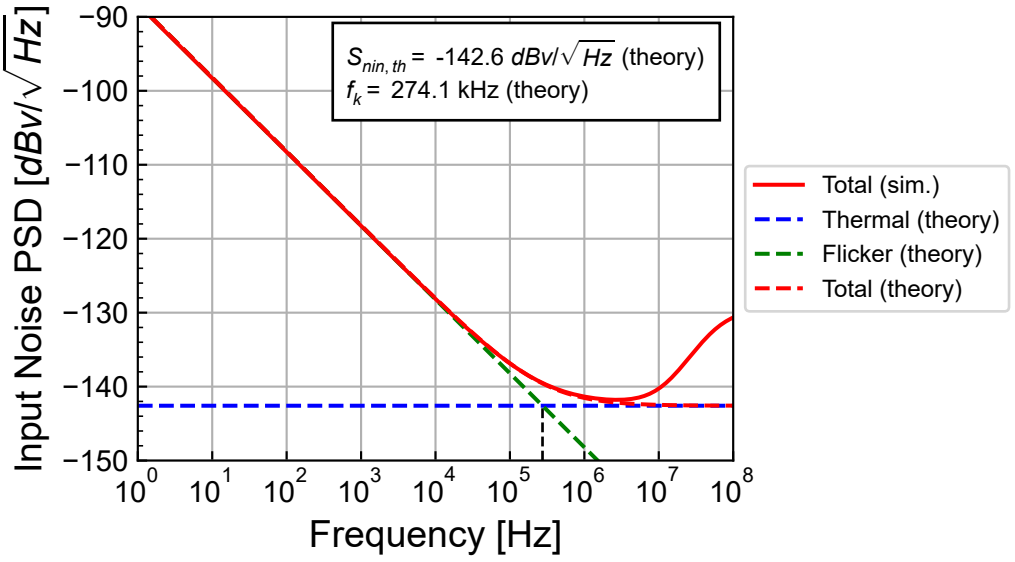

Figure 5.5: Simulated input-referred noise PSD compared to theoretical estimation.

larger than the theoretical estimation. This is simply due to the fact that the input-referred noise PSD has been obtain by dividing the output current noise by the square of the equivalent trnasconductance without accouting for the frequency dependence occuring above the GBW.

The contributions of M_{1a}-M_{1b}, M_{2a}-M_{2b}-M_{2c}-M_{2d}, M_{3a}-M_{3b} and the cascode transistors M_4 and M_7 to the input-referred white noise PSD are detailed in Figure 5.6 and compared to the theoretical white noise.

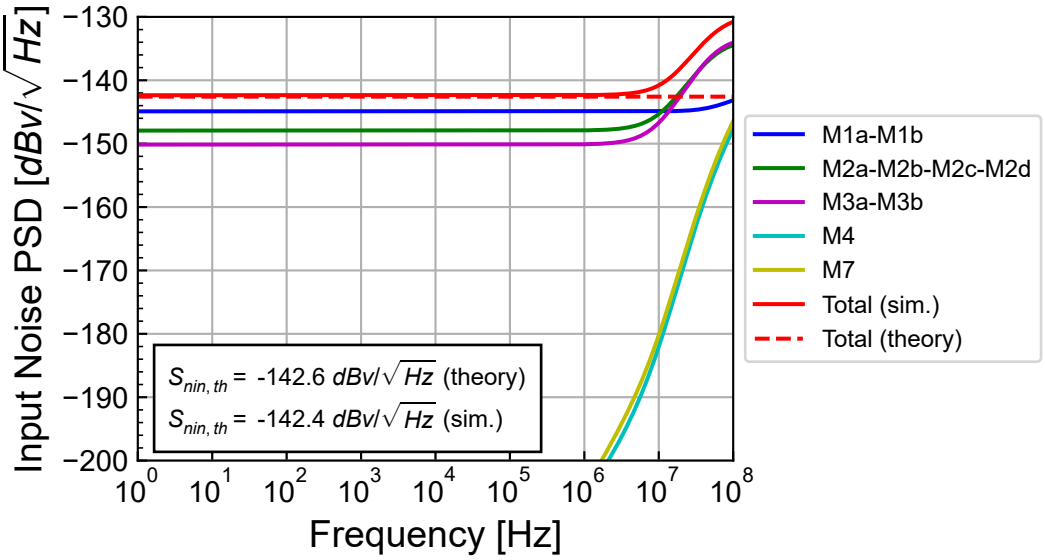

Figure 5.6: Breakdown of the contributions to the simulated input-referred white noise PSD.

From Figure 5.6, we can observe a perfect match of the total input-referred white noise PSD between simulation and the theoretical estimation. The white noise is dominated by the differential pair M_{1a}-M_{1b} which is $1 + \eta_{th} = 1.796$ times (or 2.544 dB) lower than the total white noise. The contribution of M_{2a}-M_{2b}-M_{2c}-M_{2d} is about 2.011 times (or 3.033 dB) lower than the contribution of M_{1a}-M_{1b}. The contribution of M_{3a}-M_{3b} is about 3.345 times (or 5.243 dB) lower than the contribution of M_{1a}-M_{1b}. Finally, the contributions of the cascode transistors M_4 and M_7 are completely negligible. (65.682 dB lower for M_4 and 74.893 dB lower for M_7). This confirms that the noise of the cascode transistors M_4 and M_7 can be totally neglected.

The simulated value of $\eta_{th} = 0.796$ is almost equal to the theoretical estimation $\eta_{th} = 0.775$. Finally, the simulated OTA thermal noise excess factor $\gamma_{n,ota} = 2.416$ is slightly larger than the predicted value $\gamma_{n,ota} = 2.319$.

Figure 5.7 presents the breakdown of the contributions of the various transistors to the input-referred flicker noise. As expected from the design, M_{2a}-M_{2b}-M_{2c}-M_{2d} contribute about the same than M_{1a}-M_{1b}.

The breakdown of the contributions of the various transistors to the total input-referred noise is presented in Figure 5.8. We can observe that the simulation is slightly larger than the theoretical estimation.

5.5 Input common-mode voltage range

We can check the input common-mode voltage range by connecting the OTA as a voltage follower and sweeping the positive input. The result is shown in Figure 5.9.

As shown in Figure 5.9, the output follows the input voltage up to 1.45 V. So the input common-mode voltage range is about 1.45 V.

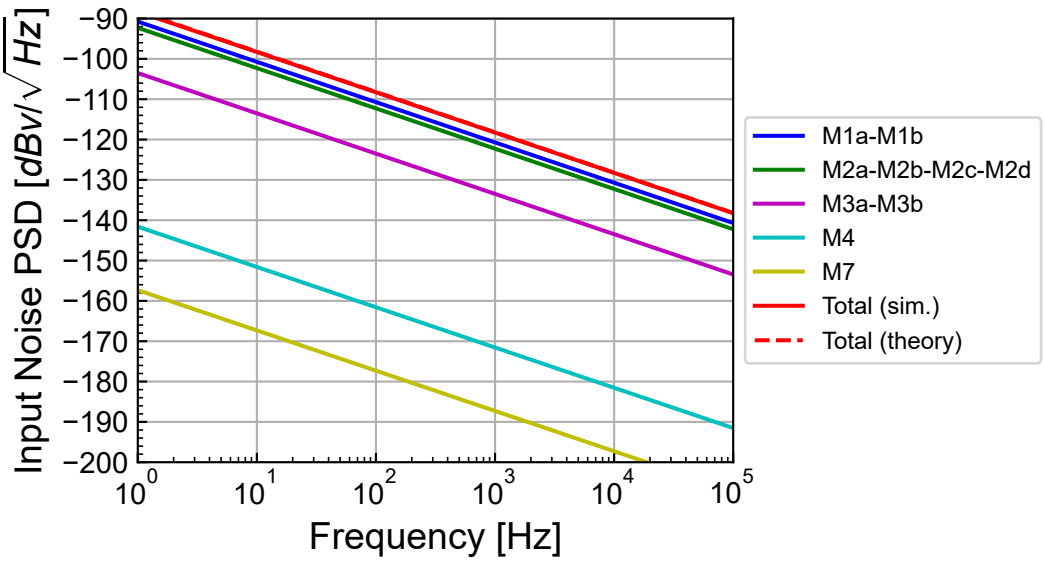

Figure 5.7: Breakdown of the contributions to the simulated input-referred flicker noise PSD.

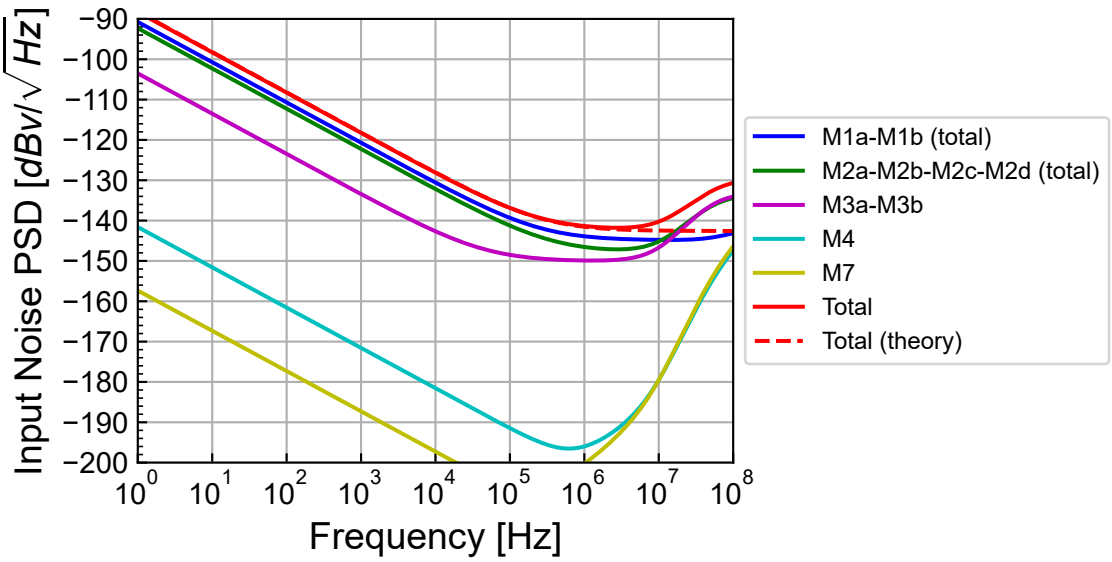

Figure 5.8: Breakdown of the contributions to the simulated input-referred noise PSD.

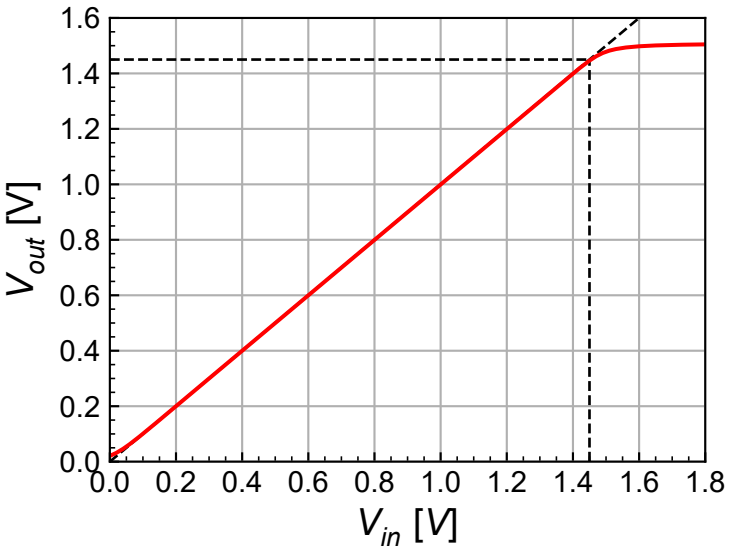

Figure 5.9: Simulated input common-mode voltage range.

5.6 Step-response

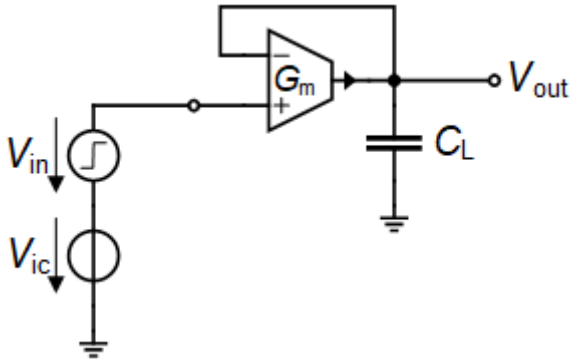

Figure 5.10: Schematic of the OTA connected as a voltage follower.

In this section we will check the step response of the OTA operating as a voltage follower as shown in Figure 5.10 with its output connected to the negative input and with the same load capacitance $C_L = 1\ pF$.

5.6.1 Small-step

We start by imposing a small step $\Delta V_{in} = 10\ mV$ on top of a common mode voltage $V_{ic} = 0.9\ V$. The simulation results are shown in Figure 5.11 where $\Delta V_{in}(t) \triangleq V_{in+}(t) - V_{ic}$ and $\Delta V_{out}(t) \triangleq V_{out}(t) - V_{outq}$ with V_{outq} the quiescent output voltage at the operating point before the step is applied. ΔV_{in} and ΔV_{out} are compared to the response of a single pole circuit having a cut-off frequency equal to the GBW. The difference between the simulation an the first-order model is due to the larger estimated value of the GBW and the additional poles introduced by the current mirrors.

5.6.2 Large step

We now impose a larger step $\Delta V_{in} = 300\ mV$ on top of a common mode voltage $V_{ic} = 400\ mV$. The simulation results are shown in Figure 5.12 where $\Delta V_{in}(t) \triangleq V_{in+}(t) - V_{ic}$ and $\Delta V_{out}(t) \triangleq V_{out}(t) - V_{outq}$ with $V_{outq} \cong V_{ic}$ the quiescent output voltage at the operating point before the step is applied. ΔV_{in}

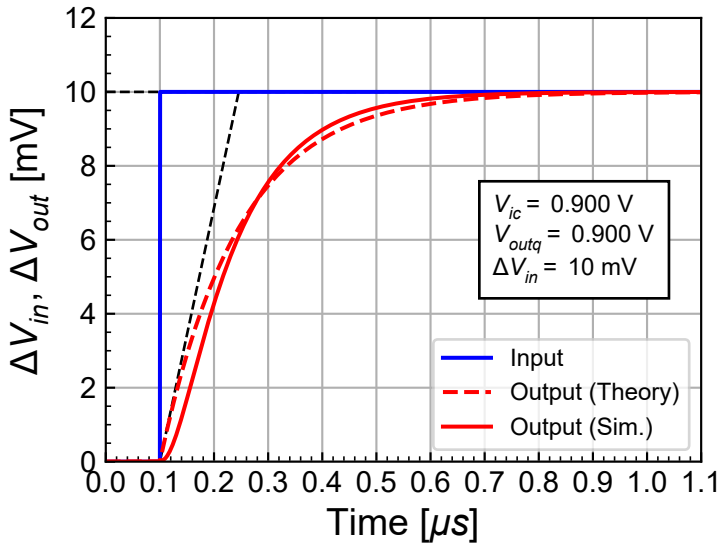

Figure 5.11: Step response of the OTA as a voltage follower for a small input step.

and ΔV_{out} are compared to the response of a single pole circuit having a cut-off frequency equal to the GBW. We now observe the effect of slew-rate which increases the settling time.

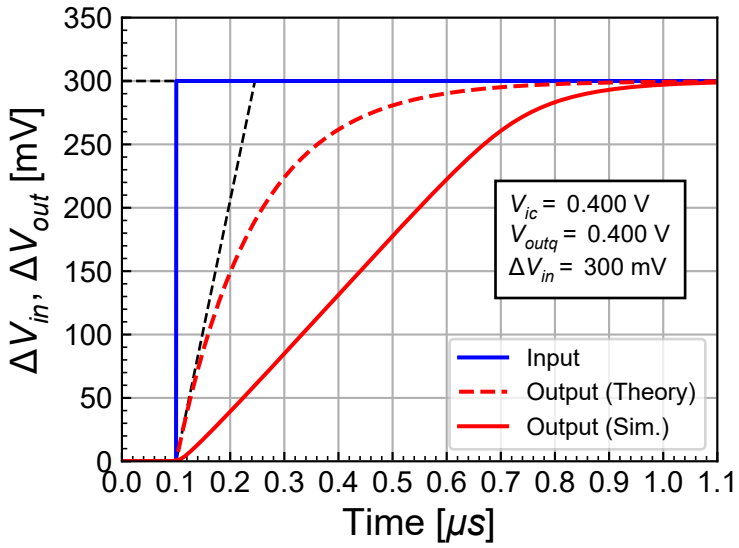

Figure 5.12: Step response of the OTA as a voltage follower for a large input step highlighting the slew-rate effect.

5.7 Current and power consumption

The total current consumption (without accounting for the current in M_{5a}) is given by $I_{tot} = 1.000$ μA, resulting in a total power consumption given by $P = 1.800$ μW. We can compare the current and power consumption of the Miller OTA to the telescopic OTA $I_{tot,telescopic} \cong 0.5$ μA. The current and power consumption of the symmetrical cascode OTA is 2.000 times larger than that of the telescopic OTA for similar specifications and performance.

6 Conclusion

This notebook presented the analysis, design and verification of the symmetrical cascode OTA [1] designed for a generic 180nm bulk CMOS process. The detailed analysis provided all the equations that were then used in the design phase to reach the target specifications. The design was then performed using the inversion coefficient approach with the sEKV transistor model [2] [3] [4]. The theoretical performance resulting from the design were then evaluated.

The design was then verified by simulation using ngspice [5] with the EKV 2.6 compact model [6] and the parameters of a generic 180 nm bulk CMOS process. Because of the high output resistance and the structural mismatch in the current mirrors due to the output conductances, the open-loop quiescent output voltage was too low, pushing some transistors out of saturation. The OTA was then simulated in closed-loop as a voltage follower in order to extract the offset voltage required to bring the quiescent output voltage in open-loop back to the high gain region. After carefully checking the operating point, the large-signal transfer characteristic was simulated. Then the small-signal transfer function of the OTA connected as a voltage follower was simulated. The open-loop transfer function was then simulated making sure the OTA was biased in the high gain region. The transfer function was then compared to the that extracted from the closed-loop simulation showing a reasonable correspondance below the unity gain frequency. The simulations have shown that the gain-bandwidth product GBW and the DC gain are both achieved.

The input-referred noise was then simulated showing results that are very close to the theoretical estimation for both the white noise and the flicker noise. The contributions of the various transistors to the input-referred white noise were then extracted from the noise simulation and compared to the theoretical estimation. It was shown that the total white noise is very close to the theoretical estimation. It was then shown that the flicker noise of the current mirrors is about equal to that of the differential pair. Finally, the simulations have confirmed that the noise contributions of the cascode transistors are completely negligible.

The input common-mode voltage range was then simulated with the OTA connected as a voltage follower.The input voltage is limited to $1.4\,V$.

Finally, the small-signal step response was simulated and succesfully compared to the response of a single-pole system. The step-response with a large input step highlighted the effect of slew-rate.

References

[1] F. Krummenacher, "High voltage gain CMOS OTA for micropower SC filters," *Electronics Letters*, vol. 17, no. 4, pp. 160–162, 1981.

[2] C. C. Enz and E. A. Vittoz, *Charge-Based MOS Transistor Modeling - The EKV Model for Low-Power and RF IC Design*, 1st ed. John Wiley, 2006.

[3] C. Enz, F. Chicco, and A. Pezzotta, "Nanoscale MOSFET Modeling: Part 1: The Simplified EKV Model for the Design of Low-Power Analog Circuits," *IEEE Solid-State Circuits Magazine*, vol. 9, no. 3, pp. 26–35, 2017.

[4] C. Enz, F. Chicco, and A. Pezzotta, "Nanoscale MOSFET Modeling: Part 2: Using the Inversion Coefficient as the Primary Design Parameter," *IEEE Solid-State Circuits Magazine*, vol. 9, no. 4, pp. 73–81, 2017.

[5] Holger Vogt, Giles Atkinson, Paolo Nenzi, "Ngspice User's Manual Version 43." https://ngspice.sourceforge.io/docs/ngspice-43-manual.pdf, 2024.

[6] M. Bucher, C. Lallement, C. Enz, F. Théodoloz, and F. Krummenacher, "The EPFL-EKV MOSFET Model Equations for Simulation." https://github.com/chrisenz/EKV/blob/main/EKV2.6/docs/ekv_v26_rev2.pdf, 1998.

[7] M. Bucher, C. Lallement, C. Enz, F. Théodoloz, and F. Krummenacher, "EKV 2.6 Verilog-A Code." https://github.com/chrisenz/EKV/tree/main/EKV2.6/va/code, 2024.

[8] W. Grabinski *et al.*, "FOSS EKV2.6 verilog-a compact MOSFET model," in *European solid-state device research conference (ESSDERC)*, 2019, pp. 190–193. doi: 10.1109/ESSDERC.2019.8901822.

[9] W. Grabinski *et al.*, "FOSS EKV 2.6 parameter extractor," in *2015 22nd international conference mixed design of integrated circuits & systems (MIXDES)*, 2015, pp. 181–186. doi: 10.1109/MIXDES.2015.7208507.

[10] Han, H.-C. and A. D'Amico and C. Enz, "SEKV-E: Parameter Extractor of Simplified EKV I-V model for Low-power Analog Circuits." https://gitlab.com/moscm/sekv-e, 2022.

[11] F. Krummenacher, E. Vittoz, and M. Degrauwe, "Class AB CMOS amplifier micropower SC filters," *Electronics Letters*, vol. 17, no. 13, pp. 433–435, 1981.

[12] M. G. Degrauwe, J. Rijmenants, E. A. Vittoz, and H. J. D. Man, "Adaptive biasing CMOS amplifiers," *IEEE Journal of Solid-State Circuits*, vol. 17, no. 3, pp. 522–528, 1982.

[13] C. C. Enz, F. Krummenacher, and E. A. Vittoz, "An Analytical MOS Transistor Model Valid in All Regions of Operation and Dedicated to Low-Voltage and Low-Current Applications," *Analog Integrated Circuits and Signal Processing Journal*, vol. 8. https://github.com/chrisenz/EKV/tree/main/EKV2.6/docs/EKV_original_paper_1995_prepub.pdf, pp. 83–114, 1995.

[14] Dietmar Warning, "Verilog-A Models for Circuit Simulation." https://github.com/dwarning/VA-Models, 2024.

[15] SemiMod GmbH, "Open VAF." https://openvaf.semimod.de/docs/getting-started/introduction/, 2025.